

Dynamically assisted tunneling in the Floquet picture

Daniil Ryndyk,¹ Christian Kohlfürst^{1,*}, Friedemann Queisser,¹ and Ralf Schützhold^{1,2}

¹*Helmholtz-Zentrum Dresden-Rossendorf, Bautzner Landstraße 400, 01328 Dresden, Germany*

²*Institut für Theoretische Physik, Technische Universität Dresden, 01062 Dresden, Germany*

 (Received 13 October 2023; revised 31 January 2024; accepted 12 March 2024; published 16 April 2024)

We study how tunneling through a potential barrier $V(x)$ can be enhanced by an additional harmonically oscillating electric field $\mathcal{E}(t) = \mathcal{E}_0 \cos(\omega t)$ or a similar oscillating force. To this end, we transform into the Kramers-Henneberger frame and calculate the coupled Floquet channels numerically. We find distinct signatures of resonances when the incident energy E equals the driving frequency $\omega = E$, which clearly shows the breakdown of the time-averaged potential approximation in this regime. As a simple model for experimental applications (e.g., in solid-state physics), we study the rectangular potential, which can also be benchmarked with respect to analytical results. Finally, we consider the truncated Coulomb potential relevant for nuclear fusion.

DOI: [10.1103/PhysRevResearch.6.023056](https://doi.org/10.1103/PhysRevResearch.6.023056)

I. INTRODUCTION

Quantum tunneling is ubiquitous in physics. It plays an important role in many areas, such as ultracold atoms in optical lattices [1–8], electrons in solid-state devices [9–15], field ionization in atomic physics [16–20], as well as nuclear α -decay, proton emission, and fusion [21–26], to name only a few examples; see also Refs. [27,28]. However, even though tunneling through a static potential barrier $V(x)$ is usually taught in the basic lecture course on quantum mechanics, our understanding of tunneling in time-dependent scenarios such as $V(x, t)$ is still far from complete. As one example, let us mention the recent controversy on the dynamical assistance of nuclear α -decay [29–34].

If the temporal variation of the potential $V(x, t)$ is very slow, the problem can be treated via the quasistatic potential approximation by calculating tunneling as for a static potential barrier (at each instant of time). On the other hand, if the potential $V(x, t)$ changes from an initial $V_{\text{in}}(x)$ to a final form $V_{\text{out}}(x)$ in a very short time, we may use the sudden approximation by evolving the initial wave function $\psi_{\text{in}}(x)$ in the final potential $V_{\text{out}}(x)$. Extremely rapidly oscillating potentials $V(x, t)$ can often be dealt with in the time-averaged potential approximation, where the time-dependent potential is replaced by its time average $\bar{V}(x) = \overline{V(x, t)}$.

However, away from these extreme cases, one may discover many nontrivial and fascinating phenomena [35–41], including resonance [42,43] or assistance effects [44–48]. Furthermore, the regions of validity of the aforementioned approximations is also a nontrivial question. In this respect,

the Landauer-Büttiker “traversal” time [49] plays an important role in separating slow (i.e., adiabatic) from fast (i.e., nonadiabatic) processes.

In the following we study the possible enhancement of tunneling by an additional time dependence, referred to as “dynamically assisted tunneling.” Instead of a fully general space-time-dependent potential $V(x, t)$, we consider a static barrier $V(x)$ with an additional force which is harmonically oscillating in time. For the charged particles considered here, this force could be generated by a harmonically oscillating electric field $\mathcal{E}(t) = \mathcal{E}_0 \cos(\omega t)$. For neutral particles such as atoms in optical lattices, shaking the lattice or applying suitable time-dependent magnetic or optical potentials would have the same effect. The work here can be regarded as a logical continuation of our previous publication [50], where we considered pulsed electric fields and identified nonadiabatic enhancement effects. The generalization to oscillating fields $\mathcal{E}(t) = \mathcal{E}_0 \cos(\omega t)$ allows us to study resonance effects and to apply our findings to more experimentally relevant scenarios.

Note that we restrict our considerations to the directly measurable tunneling probability and its increase, but we do not address the question of the “tunneling time,” i.e., how long the particle actually stays inside the barrier [49,51–56]. This intriguing question is sometimes also discussed in this context and turns out to be quite nontrivial—already at the level of a proper definition.

To study the enhancement of tunneling, we transform into the Kramers-Henneberger frame and employ Floquet theory to split the system into a set of coupled channels, see Sec. II. As our first application, we consider the rectangular potential in Sec. III, which serves as a simple model for experimental applications in solid-state physics, such as scanning tunneling microscopy (STM) or tunneling through insulating layers. As our second application, we study the truncated Coulomb potential in Sec. IV, which is relevant for nuclear fusion. However, as tunneling phenomena play an important role in many areas, our main results should also be applicable in other cases, see also Secs. VI and V.

*Corresponding author: c.kohlfuerst@hzdr.de

Published by the American Physical Society under the terms of the [Creative Commons Attribution 4.0 International](https://creativecommons.org/licenses/by/4.0/) license. Further distribution of this work must maintain attribution to the author(s) and the published article's title, journal citation, and DOI.

II. THEORETICAL FORMALISM

Our aim in this paper is to study time-dependent, nonrelativistic assisted quantum tunneling. As such, the fundamental dynamics of our quantum system is very well governed by the following Schrödinger equation:

$$i\hbar \frac{\partial}{\partial t} \psi(x, t) = \hat{H}(x, t) \psi(x, t), \quad (1)$$

with Schrödinger Hamiltonian \hat{H} and wave function ψ . For the purposes of this research, we restrict ourselves to a single particle (without internal structure) in a one-dimensional spatial domain in order to limit the rich configuration space.

We want to further assume that our test particle has a defined energy E in its initial state. We choose this particular approach as it gives us a clear picture of the tunneling probability for a specific energy and provides us with simple expressions regarding general scaling laws. Additionally, a focus on individual energy modes makes it easier to relate our findings to discussions on simpler systems, such as the well-known tunneling probability in static problems [57]:

$$P \sim \exp\left[-2 \int dx \sqrt{2\mu[V(x) - E]/\hbar}\right], \quad (2)$$

with energy E , mass μ , and barrier $V(x)$. For complementary discussions of assisted tunneling with respect to wave packets, we refer to Refs. [50,58,59].

Another advantage of focusing on individual modes is that expanding the formalism from static to time-periodic problems is attainable with relatively little effort, see also Refs. [60,61].

In this article we discuss results for a subclass of time-dependent potentials [62]. In particular, we are interested in quantum tunneling in the presence of a linearly polarized, oscillating field as described by the vector potential

$$A(t) = -\frac{\mathcal{E}_0}{\omega} \sin(\omega t). \quad (3)$$

As in many other cases, it is advantageous to study such a periodically driven quantum system in Floquet theory [27,63], which is a means of transforming an explicit time-dependent problem into a time-independent one. The cost comes in the form of an extended Hilbert space, as multiple energy modes have to be considered within one calculation.

In this case energy is not conserved anymore, and by means of minimal coupling, $\hat{p} \rightarrow \hat{p} - qA(t)$ with charge q , a sinusoidal field directly leads to discrete mode coupling, i.e., interaction between the Floquet channels. More precisely, we see the formation of sidebands of energy $E \pm n\omega$ with n integer, see Refs. [27,64] or for the related Franz-Keldysh effect [65,66].

A. Kramers-Henneberger transformation

For a static scalar potential $V(x)$ but time-dependent vector potential $A(t)$, the Hamiltonian reads ($\hbar = c = 1$)

$$\hat{H}(t) = \frac{[\hat{p} - qA(t)]^2}{2\mu} + V(\hat{x}). \quad (4)$$

However, in the following we shall work in a different representation. Similar to the locally freely falling frame, in which

the gravitational acceleration is transformed away, we go to the Kramers-Henneberger frame where the vector potential $A(t)$ is transformed away. The price to pay is a time dependence of the new potential $V(x, t)$.

The basic idea is that on the basis of the laboratory frame we make an ansatz for the wave function [67],

$$\begin{aligned} \psi(x, t) = & \exp\left(-\frac{iq^2}{2\mu} \int_0^t dt' A^2(t')\right) \\ & \times \exp\left(\frac{q}{\mu} \int_0^t dt' A(t') \partial_x\right) \psi_{\text{KH}}(x, t), \end{aligned} \quad (5)$$

where ψ_{KH} is the wave function in the transformed system. Then, instead of having the wave function being affected by the translation operator in the second line, we can choose the coordinate system that automatically follows the new wave function, with the result that the translation operator then applies to the potential. This removes any explicit reference to the vector potential $A(t)$ and converts any field-induced motion into the outcome of a moving scalar barrier $V(x, t)$. Consequently, the Schrödinger equation reads

$$\begin{aligned} i\hbar \frac{\partial}{\partial t} \psi_{\text{KH}}(x, t) \\ = \left(-\frac{1}{2\mu} \frac{\partial^2}{\partial x^2} + V[x - \chi(t)]\right) \psi_{\text{KH}}(x, t), \end{aligned} \quad (6)$$

where the displacement $\chi(t)$ satisfies the classical equation of motion,

$$\mu \ddot{\chi}(t) = q\dot{A}(t), \quad (7)$$

for a point-particle in a time-dependent external field.

The mathematics behind this change in reference frame is provided in Appendix A 1. Further note the difference between a potential moving in spatial direction and a scalar potential of modulated height [68–70]. Actually, for the case of ultracold atoms in optical lattices mentioned in the Introduction, where the oscillating electric field is replaced by shaking the lattice, the Kramers-Henneberger transformation has a direct interpretation as it transforms between the inertial frame and the accelerated rest frame of the lattice.

Working in the Kramers-Henneberger frame has several advantages. On the one hand, it is more intuitive as we only have to account for a single rigid potential with a time-dependent displacement. On the other hand, for spatially localized potential barriers, the effect of the time-dependent electric field is also spatially localized. In contrast, the time dependence of the original Hamiltonian (4) applies to all space points in the same way. Even worse, the representation of the electric field $\mathcal{E}(t)$ via the potential $\mathcal{V}(x, t) = xq\mathcal{E}(t)$ would result in a “perturbation” which increases without bound at spatial infinity.

B. Floquet theory

As already mentioned above, the treatment of periodic time dependences can be simplified by a Floquet expansion. This allows us to factor out the time evolution and to reduce the Schrödinger equation (6) from a partial differential equation in t and x to a system of ordinary differential equations in x . To do so we expand the wave function into an unperturbed

part times a Fourier decomposition,

$$\psi_{\text{KH}}(x, t) = e^{-iEt} \sum_{n=-\infty}^{\infty} u_n(x) e^{in\omega t}, \quad (8)$$

and, following the same principle, we also decompose the new scalar potential into Fourier modes:

$$V(x, t) = V[x - \chi(t)] = \sum_{n=-\infty}^{\infty} V_n(x) e^{in\omega t}. \quad (9)$$

The resulting equations do not exhibit an explicit time dependence anymore:

$$\frac{d^2}{dx^2} u_n(x) + k_n^2 u_n(x) = \sum_{m=-\infty}^{\infty} v_{nm}(x) u_m(x), \quad (10)$$

with $k_n \equiv \sqrt{2\mu(E + n\omega)}$ and $v_{nm}(x) \equiv 2\mu V_{n-m}(x)$. Thus, instead of solving a partial differential equation in x and t , we solve a system of mode-coupled, ordinary differential equations in x only.

For the sake of simplicity, we will assume that we integrate over a sufficiently large spatial interval such that any given scalar potentials have either become zero or have fallen off substantially at the boundaries of integration. In this case we can assume that mode functions become decoupled plane waves asymptotically.

C. Coupled-channels formulation

The coupled set of ordinary second-order differential equations (10) with boundary conditions at $x \rightarrow +\infty$ and $x \rightarrow -\infty$ is still not the best option for a numerical integration. Thus, let us transform this set (10) into a set of first-order differential equations corresponding to an initial-valued problem; see also Ref. [28] and Appendix A 2. As the first step, we use the Green's function $G_n(x, x') = \exp\{ik_n|x - x'|\}/(2ik_n)$ of the differential operator in Eq. (10) in order to reformulate Eq. (10) as a coupled set of integral equations,

$$u_{nl}(x) = e^{ik_n x} \delta_{nl} + \sum_{m=-\infty}^{\infty} \int_{-\infty}^{\infty} dx' G_n(x, x') v_{nm}(x') u_{ml}(x'), \quad (11)$$

where we have added a homogeneous solution $e^{ik_n x}$ of the differential operator in Eq. (10) and introduced an additional index l as a label for the initial Floquet channel. This homogeneous solution accounts for the boundary condition that there are only incoming waves from the left, where the δ_{nl} ensures that we have only waves with the wave number k_l of the initial Floquet channel. Instead of solving Eq. (11) directly, we introduce an auxiliary variable y with the intention to progressively probe the full potential:

$$u_{nl}(x, y) = e^{ik_n x} \delta_{nl} + \frac{1}{2ik_n} \sum_{m=-\infty}^{\infty} \int_y^{\infty} dx' e^{ik_n|x-x'|} v_{nm}(x') u_{ml}(x', y). \quad (12)$$

Taking y derivatives and using the fact that we are only interested in the asymptotic limits $x \rightarrow \pm\infty$, we may map the set

of integral equations (11) onto a set of ordinary differential equations in y in terms of y -dependent quasi-transmission and quasi-reflection amplitudes (see also Ref. [28] and Appendix A 2):

$$\frac{d}{dy} \rho_{nl}(y) = - \sum_{s=-\infty}^{\infty} \frac{1}{2ik_s} (e^{ik_s y} \delta_{ns} + \rho_{ns}(y) e^{-ik_s y}) \times \sum_{m=-\infty}^{\infty} v_{sm}(y) (e^{ik_m y} \delta_{ml} + \rho_{ml}(y) e^{-ik_m y}), \quad (13)$$

$$\frac{d}{dy} \tau_{nl}(y) = - \sum_{s=-\infty}^{\infty} \frac{1}{2ik_s} (e^{-ik_s y} \delta_{ns} + \tau_{ns}(y) e^{-ik_s y}) \times \sum_{m=-\infty}^{\infty} v_{sm}(y) (e^{ik_m y} \delta_{ml} + \rho_{ml}(y) e^{-ik_m y}). \quad (14)$$

This coupled set of equations is now more suitable for numerical integration. According to Eq. (12), we are interested in the behavior at $y \rightarrow -\infty$, while the other limit $y \rightarrow \infty$ becomes trivial, leading to the initial conditions $\rho_{nl}(y \rightarrow \infty) = 0$ and $\tau_{nl}(y \rightarrow \infty) = 0$. Thus, we have to integrate Eqs. (13) and (14) backwards from $y \rightarrow \infty$ to $y \rightarrow -\infty$. As an intuitive picture, the $\tau_{nl}(y)$ and $\rho_{nl}(y)$ tell us how much amplitude is transmitted (τ_{nl}) or reflected (ρ_{nl}) from the initial Floquet channel l into the final Floquet channel n up to the spatial point y .

In the asymptotic limit we recover the transmission T_{nl} and reflection R_{nl} amplitudes for the various channels:

$$T_{nl} = \delta_{nl} + \tau_{nl}(y \rightarrow -\infty), \quad R_{nl} = \rho_{nl}(y \rightarrow -\infty). \quad (15)$$

More precisely, the probability for a mode of initial energy E_l to become a transmitted or reflected mode with final energy E_n is given by $|T_{nl}|^2 k_n/k_l$ or $|R_{nl}|^2 k_n/k_l$, respectively. It should be noted, however, that this relation is only valid for matter waves with real and positive wave vectors k_n and k_l .

In the following we focus on the transmission amplitudes T_{nl} . However, the formalism can also be used to study the reflective properties of a potential, see Sec. VI below. A detailed derivation of the formalism can be found in Appendix A 2. For a more detailed review, see Ref. [28]. Computational solution techniques, error analysis, as well as the performance and efficiency of the used solver are discussed in Ref. [71].

III. RECTANGULAR POTENTIAL

We first consider scattering at a rectangular potential:

$$V(x) = \begin{cases} 0 & \text{for } x \leq 0, \\ V_0 > 0 & \text{for } 0 < x < L, \\ -V_1 & \text{for } x \geq L, \end{cases} \quad (16)$$

of height V_0 and length L . The asymptotic potential levels before and after the barrier can be different, given by the offset V_1 . This potential (16) can be considered as a one-dimensional toy model for STM, where the region $x \leq 0$ corresponds to the tip and the region $x \geq L$ to the substrate, while the interval $0 < x < L$ models the vacuum in between. As another application, the potential could describe tunneling through an insulating layer between two conductors.

As a standard textbook example of quantum tunneling, the rectangular potential is particularly interesting as a toy model. In the static case, the exact reflection and transmission coefficients are well known. In the dynamic case of assisted tunneling, especially in the Kramers-Henneberger framework, the physical implications of having an additional external field present can be understood intuitively. The lack of an internal structure in V_0 and the clear separation between regions (before, after, and inside the barrier) are features that are quite beneficial for computational techniques and even facilitate analytical results in various limiting cases, see Appendixes B 1–B 4.

Before discussing the results for the rectangular potential, let us briefly recapitulate how an electric field $\mathcal{E}(t)$ could enhance (or suppress) tunneling. Trying to separate the different effects, one can identify at least four main contributions, see also Ref. [50]. Even if we ignore the time dependence of the electric field \mathcal{E} , it can accelerate (or decelerate) the particle before it hits the barrier (*preacceleration*) and thereby enhance (or suppress) tunneling, or it can effectively deform the barrier (*deformation*). Apart from these two adiabatic effects, the time dependence of $\mathcal{E}(t)$ induces a coupling of the Floquet channels, leading to an effectively higher (or lower) energy $E \rightarrow E \pm n\omega$. This *energy mixing* is most effective at the front end of the barrier. In addition, the Kramers-Henneberger *displacement* is most effective at the rear end of the barrier, where it can liberate the wave packet inside the barrier and thereby enhance tunneling.

A. Resonance effects

Let us now present the numerical results for the rectangular potential, obtained by solving Eqs. (13) and (14) for the coupled Floquet channels. The relative enhancement, i.e., dynamically assisted transmission probability divided by the value without the field $\mathcal{E}(t)$, is plotted in Fig. 1 for a specific barrier size and field strength, and three values for the offset V_1 .

As a first result, we do see a significant enhancement of the tunneling probability for the chosen set of parameters. For other parameters (e.g., higher field strengths \mathcal{E}_0), the enhancement can be even more pronounced, but this typically requires taking into account more Floquet channels and is thus numerically more demanding.

As a second result, we observe resonance effects in the form of peaks or cusps at $E = \omega$ and $E = \omega - V_1$. These features clearly show that the time-averaged potential approximation cannot be applied here, which is, perhaps, not too surprising since the driving frequency ω is not much larger than all other relevant scales. Furthermore, the nonmonotonic dependence on E indicates that this feature also cannot be explained by the adiabatic preacceleration and potential deformation effects mentioned above. The resonance effects are of nonadiabatic origin and occur when a Floquet channel opens up or closes in one or both of the asymptotic regions. The dependence on V_1 shows that energy mixing at the front end is probably not the only relevant mechanism here, the displacement (which also occurs at the rear end) must also be relevant. Quite intuitively, the Floquet channel that opens up or closes corresponds to a very large wavelength outside

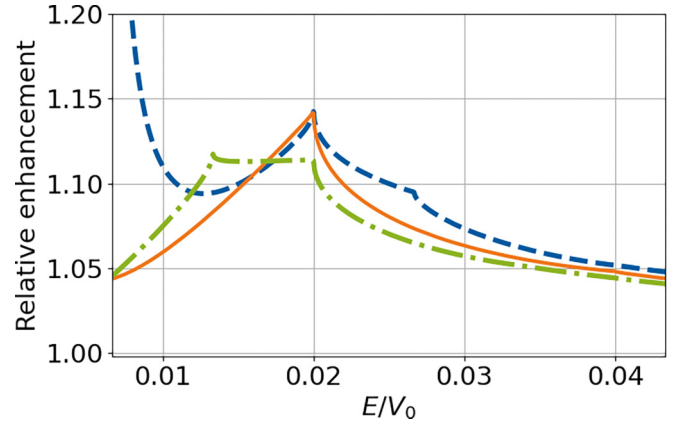


FIG. 1. Relative enhancement in the electron transmission probability through a rectangular barrier as a function of initial energy E for different asymptotic levels V_1 . The blue, dashed curve corresponds to tunneling through a barrier where the potential behind the barrier is higher than the initial potential $V_1/V_0 = -0.007$. The green dot-dashed curve shows tunneling through a barrier with a lower-laying asymptotic potential $V_1/V_0 = +0.007$. The orange, solid line holds as a reference where asymptotic levels are equal, $V_1 = 0$. One resonance appears where the incident energy E of the matter wave and the driving frequency ω coincide. The second peak appears around energies of $E = \omega - V_1$. Note that the blow-up of the blue, dashed curve at $E = -V_1$ is a result of the normalization, since the undisturbed tunneling probability (without the electric field) vanishes for $E \leq -V_1$ due to energy conservation. Parameters: barrier width $L = 2.45/\sqrt{2\mu V_0}$ and field strength $\mathcal{E}_0 = 0.008 V_0/(qL)$. For electrons in vacuum (e.g., in a STM), these values can be realized via $V_0 = 6$ eV, $L = 0.2$ nm, and $\mathcal{E}_0 = 2.4 \times 10^8$ V/m, for example.

the barrier, which makes it very susceptible to these nonadiabatic effects. This is true even for evanescent waves near the threshold, which can make a significant contribution to the transmission probability if the corresponding energy band is populated and the probability is consequently transferred to an outgoing wave.

A closer inspection of Fig. 1 reveals higher-order resonances at $E = 2\omega$, but as they are hard to see, we plotted another set of parameters in Fig. 2 with special emphasis on second-order resonances.

B. Sidebands

Now, after having discussed the total transmission probability, let us study the contributions of the sidebands, where we focus on the first two sidebands $E \pm \omega$ for simplicity, as shown in Fig. 3 for vanishing offset $V_1 = 0$.

The lower sideband at $E - \omega$ dominates for short barriers, only for long enough barriers the upper sideband at $E + \omega$ takes over. To understand the origin for this behavior, let us first compare it to analytical approximations in the corresponding limiting cases.

For small quiver amplitudes χ_0 and short barriers, we may obtain the transmission amplitudes for the first sidebands via perturbation theory, see Appendix B 3:

$$T_{\pm 1}^{\text{transparent}} \propto (L\chi_0\mu V_0)^2 \frac{E}{E \pm \omega}. \quad (17)$$

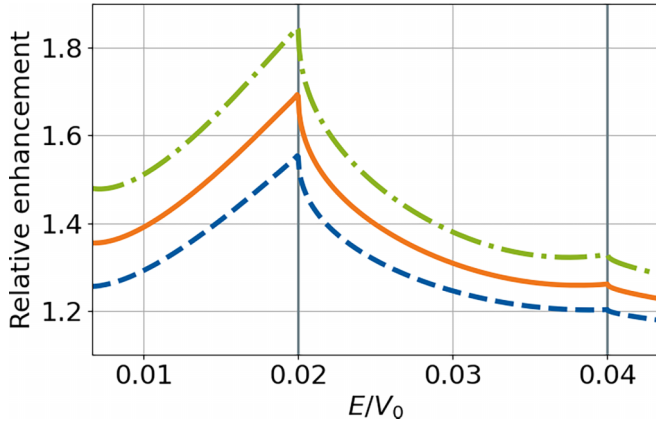


FIG. 2. Relative enhancement in the electron transmission probability through a rectangular barrier with $V_1 = 0$ as a function of initial energy E normalized by the barrier height V_0 with emphasis on higher-order resonance effects. The barrier width is given by $L = 2.45/\sqrt{2\mu V_0}$, the field frequency is fixed to $\omega/V_0 = 0.02$, and the field strengths vary between $\mathcal{E}_0 = 0.016 V_0/(qL)$ (blue, dashed), $\mathcal{E}_0 = 0.018 V_0/(qL)$ (orange, solid), and $\mathcal{E}_0 = 0.02 V_0/(qL)$ (green, dot-dashed). In terms of electrons in vacuum, the field strengths \mathcal{E}_0 correspond to values ranging from $\mathcal{E}_0 = 4.8 \times 10^8$ V/m (blue, dashed) via $\mathcal{E}_0 = 5.4 \times 10^8$ V/m (orange, solid) to $\mathcal{E}_0 = 6.0 \times 10^8$ V/m (green, dot-dashed), with field frequency $\omega = 0.12$ eV, barrier length $L = 0.2$ nm, and barrier height $V_0 = 6$ eV. Optimal relative enhancement is found at $E = \omega$ as well as $E = 2\omega$ (gray vertical lines).

This result confirms that the lower sideband dominates in this regime and points to the following intuitive interpretation: For the lower sideband, the temporal oscillation period and the

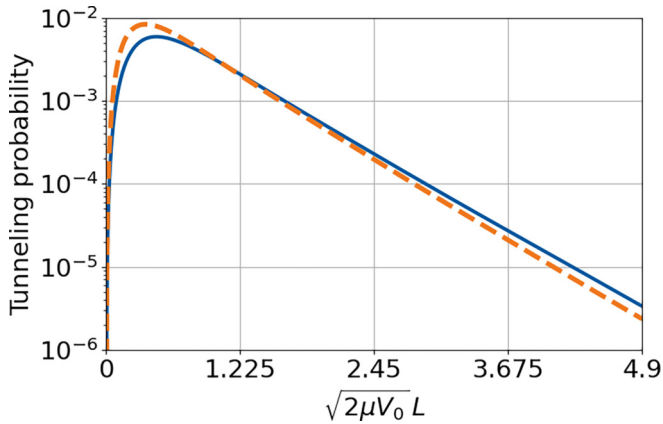


FIG. 3. The contribution of the first sidebands, $E + \omega$ (blue, solid) and $E - \omega$ (orange, dashed), towards the total tunneling probability in the context of tunneling through a rectangular barrier are displayed here in terms of $\sqrt{2\mu V_0} L$. The initial energy is given by $E/V_0 = 0.047$, with a field frequency of $\omega/V_0 = 0.02$. The peak field strength has been kept constant along the curves in the figure. At $\sqrt{2\mu V_0} L = 4.9$ we have $\mathcal{E}_0 = 0.04 V_0/(qL)$. If we consider electron tunneling in the context of an STM, the barrier height would correspond to a value of $V_0 = 6$ eV. The other relevant parameters in such a case are $\omega = 0.12$ eV, $\mathcal{E}_0 = 6 \times 10^8$ V/m, and $E = 0.28$ eV.

wavelength of the mode (outside the barrier) are longer than for the upper sideband, and thus the lower sideband is more susceptible to the Kramers-Henneberger displacement $\chi(t)$ and responds more strongly than the upper sideband.

On the other hand, the opaque-barrier limit is reached for long barriers of sufficient height $V_0 \gg \omega, E$. In this limit we obtain the approximations (see Appendix B 4)

$$T_{+1}^{\text{opaque}} \propto \frac{\chi_0 E}{V_0} (V_0 - E - \omega) e^{-2\sqrt{2\mu(V_0 - E - \omega)}L}, \quad (18)$$

$$T_{-1}^{\text{opaque}} \propto \frac{\chi_0 E}{V_0} (V_0 - E) e^{-2\sqrt{2\mu(V_0 - E)}L}. \quad (19)$$

In search for an intuitive explanation, we may understand the exponent (18) in the following way: At the front end of the barrier, the incident wave with energy E is upshifted to $E + \omega$ by the oscillating Kramers-Henneberger displacement (energy mixing) and thus can tunnel easier through the barrier, see Eq. (2). Applying the same argument to the lower sideband (19), one might expect an exponent $e^{-2\sqrt{2\mu(V_0 - E + \omega)}L}$. However, this is not the dominant contribution in this case. Instead, it stems from the central band with energy E , which tunnels through the barrier with the usual exponent $e^{-2\sqrt{2\mu(V_0 - E)}L}$ and is downshifted to $E - \omega$ at the rear end of the barrier.

In conclusion, the various bands display different dependences on the parameters, and the upper bands are not always favored over the lower-energy modes. Nevertheless, these first results already show that by pumping energy into the system, the overall probability of tunneling is typically increased in comparison to static tunneling.

C. Scaling analysis

As already mentioned in the Introduction, tunneling is ubiquitous in nature and thus our results can be applied to a variety of scenarios. In order to account for this flexibility, it is useful to discuss the physics in terms of dimensionless parameters. Then, two scenarios involving vastly different length and energy scales can still feature analogous behavior and be related to each other by rescaling, provided that the dimensionless parameters are the same.

For practical reasons, we express all energy scales relative to the potential height, i.e., in units of V_0 , yielding the three ratios E/V_0 , V_1/V_0 , and ω/V_0 . The length L of the barrier can be encoded in the dimensionless parameter $\eta = \sqrt{2\mu V_0} L$, which yields the tunneling exponent via $e^{-2\eta}$ and thus should not be too large. Note that this parameter η is also related to the Landauer-Büttiker time

$$\mathfrak{T} = L \sqrt{\frac{\mu}{2V_0}}. \quad (20)$$

More precisely, the dimensionless combination $\omega \mathfrak{T}$, which can be used to distinguish fast (i.e., nonadiabatic) $\omega \mathfrak{T} \gg 1$ from slow (i.e., adiabatic) $\omega \mathfrak{T} \ll 1$ processes, is just given by ω/V_0 times $\eta/2$. Thus, even for $\omega < V_0$, this combination $\omega \mathfrak{T}$ could be above or below unity, depending on the parameter η . As a measure of the field strength, we use the dimensionless parameter $q\mathcal{E}_0 L/V_0$ corresponding to the electrostatic energy gained over the length of the barrier.

Using these parameters in the figures, the displayed results can easily be applied to a specific experimental scenario.

To convey a feeling for the involved orders of magnitude, however, we also provide a specific example by means of an STM setup. By replacing the electron mass in vacuum with the effective electron mass in a crystal, for example, one can then rescale the results accordingly.

IV. ASSISTED NUCLEAR FUSION

Another potential application of strong-field induced assisted tunneling is in nuclear fusion [50,64,72–75]. This has already been suggested in our publication [64]. In that work [64] we focused on estimating the tunneling exponent. However, just considering the tunneling exponent may lead to an underestimate of the required field strength, as the prefactor in front of the exponential can be suppressed for a gradually increasing potential (as it is the case for the Coulomb potential), see [50]. Thus we consider the full tunneling probability, including the prefactor, in the following.

Since the characteristic length scale of tunneling is very short (in the sub-pm regime), we neglect the impact of the surrounding particles and treat nuclear fusion as a two-particle process [76]. Hence, the probability for, e.g., deuterium (D) and tritium (T) to merge can, at low temperatures, be modeled as nonrelativistic Schrödinger tunneling through the Coulomb barrier between the two positively charged particles [77–81].

Specifically, we model assisted DT fusion through nonrelativistic one-dimensional quantum mechanics, where initially we have two point-particles with masses m_D and m_T at positions r_D and r_T with velocities \dot{r}_D and \dot{r}_T , respectively. In this case, particle dynamics are given by a two-particle Lagrangian

$$\mathcal{L}_{DT} = \frac{m_D \dot{r}_D^2}{2} + \frac{m_T \dot{r}_T^2}{2} - V(|r_D - r_T|) + q\dot{r}_D A(t, r_D) + q\dot{r}_T A(t, r_T), \quad (21)$$

with kinetic terms in the first line and couplings to the potentials in the second. Hereby, $V(|r_D - r_T|)$ contains the Coulomb repulsion as well as nuclear attraction. The vector potential A corresponds, at this point, to a general electromagnetic field with a field strength shortly below the critical field strength of $E_{cr} \sim 1.3 \times 10^{18}$ V/m and a characteristic frequency in the keV regime [82].

To simplify computation, we introduce center-of-mass $R = (m_D r_D + m_T r_T)/(m_D + m_T)$ and relative coordinates $r = r_D - r_T$, respectively. Since the characteristic distances r in the sub-pm regime are much smaller than the wavelength of an x-ray field A with frequencies of order keV, we may approximate $A(t, r_D) \approx A(t, R)$ and $A(t, r_T) \approx A(t, R)$. As a result, the center-of-mass motion completely decouples from the relative coordinate r . The dynamics of assisted fusion is thus entirely described by an effective one-particle Lagrangian,

$$\mathcal{L} = \frac{\mu}{2} \dot{r}^2 - V(|r|) + q_{\text{eff}} \dot{r} A(t), \quad (22)$$

with reduced mass $\mu = (m_D^{-1} + m_T^{-1})^{-1} \approx 1.13$ GeV and effective charge $q_{\text{eff}} = q(m_T - m_D)/(m_T + m_D) \approx q/5$, while $A(t) = A(t, R)$ is effectively purely time dependent.

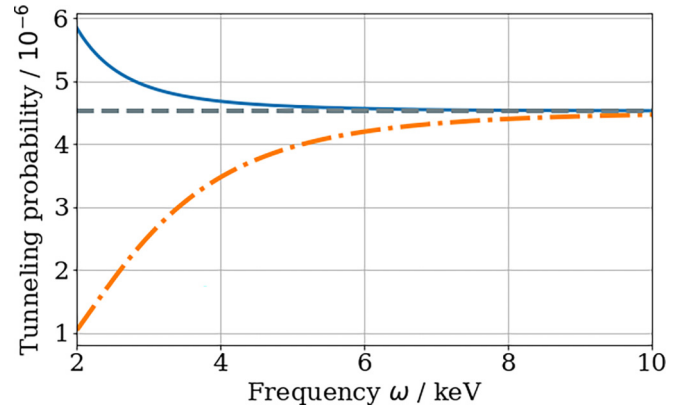


FIG. 4. Total transmission probability in a truncated Coulomb potential (23) with $V_1 = 0$ as a function of quiver frequency ω comparing the full numerical simulation (blue, solid line) with the static field-free solution (straight, gray, dashed line) and the time-averaged potential approximation (orange, dot-dashed line). The latter refers to a static potential where the quiver dynamics has been averaged over, which effectively amounts to keeping the zeroth Floquet channel only and neglecting all the others. For the blue curve a total of $N = 33$ interacting energy channels have been used. Initial energy E is 6 keV, and the field strength is $\mathfrak{E}_0 = 2 \times 10^{16}$ V/m.

The full potential is given by

$$V(r) = \begin{cases} \frac{q^2}{4\pi\epsilon_0} \frac{1}{r} & \text{for } r \geq r_0, \\ -V_1 & \text{for } r < r_0, \end{cases} \quad (23)$$

with the inner turning point $r_0 = 3.89$ fm representing the region where nuclear attraction, modeled here by a constant potential V_1 , takes over [83]. For a DT system the peak of the Coulomb potential at r_0 is roughly 375 keV. This is much larger than both the particle energies as well as the field frequencies, which are of the order of $\mathcal{O}(1 - 10)$ keV. It is much lower, however, when compared to the depth of the nuclear potential, which is in the MeV regime.

Even though analytical studies of the Coulomb potential are more involved than for the rectangular potential, the reflection and transmission amplitudes for unassisted tunneling can be obtained analytically in terms of Whittaker functions, cf. Appendix C. However, we found a direct numerical integration of the set of differential equations (13)–(14) to be faster and more accurate than evaluating the Whittaker functions.

A. Comparison to time-averaged potential

In Fig. 4 we display an exemplary result on assisted nuclear fusion. We want to place emphasis specifically on the different behavior when taking into account the full set of coupled differential equations in comparison to the time-averaged potential approximation, or equivalently, only considering the null mode in a Fourier decomposition of the Kramers-Henneberger Coulomb potential; see, also, the discussion in Refs. [84,85]. The latter is an approximation that has been widely used, for example, in laser-induced atomic stabilization because of the enormous computational simplifications it brings. For an overview, see the articles [86,87] or the review

[88] and references therein. However, for tunneling through a laterally moving barrier, as is the case in this article, Fig. 4 clearly shows that such a technical simplification leads to an incorrect tunneling probability in the low-frequency regime.

For a localized potential barrier $V[x - \chi(t)] \geq 0$ which is laterally oscillating, the above observation that the time-averaged potential approximation yields a tunneling probability which is (at least at low energies) lower than that for a static barrier $V(x)$ can be understood by the following intuitive argument: The time average leads to an effective smearing of the potential such that its effective length L_{eff} increases. At the same time, since time averaging conserves the “area” $\int dx V(x)$, the effective height V_{eff} of the potential is reduced by the same factor. Insertion into Eq. (2) shows that the increase in L_{eff} has a stronger effect on the tunneling probability (for low energies) than the reduction of V_{eff} . For larger energies near the maximum of the potential barrier, on the other hand, the reduction of the effective height V_{eff} can be the dominant effect and thus the time-averaged potential approximation can yield an enhanced tunneling probability.

The reduction of the tunneling probability predicted by the time-averaged potential approximation is the opposite of what is observed in a complete simulation where sidebands and the interaction of the main channel with the sidebands result in a net increase in transmission.

Note that the failure of the time-averaged potential approximation at low frequencies is not too surprising, since this approximation is valid when the oscillation frequency ω is much faster than all other relevant energy or frequency scales. It should also be mentioned here that going to very low frequencies becomes increasingly difficult within our scheme. On the one hand, the magnitude of the Kramers-Henneberger displacement grows as $\chi \sim 1/\omega^2$ (for fixed \mathcal{E}_0), cf. Eqs. (3) and (7). On the other hand, the distance between the Floquet channels shrinks. As a consequence, one has to take many Floquet channels into account, which becomes computationally challenging. These difficulties are related to the fact that the preacceleration effect becomes very strong for small ω , since the electric field has a long time to accelerate the particle before hitting the barrier. In this limit other approximation schemes, such as the quasistatic potential approximation, may become more adequate.

As another point, the result in Fig. 4 was obtained for vanishing offset $V_1 = 0$. Introducing such an offset $V_1 > 0$, the time-averaged potential approximation could result in a tunneling probability that is higher than in the static case, because the time-averaged potential is then reduced near its maximum. However, in this situation the applicability of the time-averaged potential approximation is even more questionable: For a reduced mass of approximately 1 GeV, a potential drop V_1 of 10 MeV or more implies that the wave packet moves away from the barrier (after tunneling) with a large velocity of around one-seventh of the speed of light or more. This is faster than the velocity of the quiver motion induced by the XFEL (with a frequency of 2 keV or more), unless field strengths above the Schwinger limit $E_{\text{cr}} \sim 1.3 \times 10^{18}$ V/m are considered. Thus, the wave packet has no chance to experience a time-averaged potential.

Note that the present investigation is focused on barrier penetration via tunneling as an effective single-particle

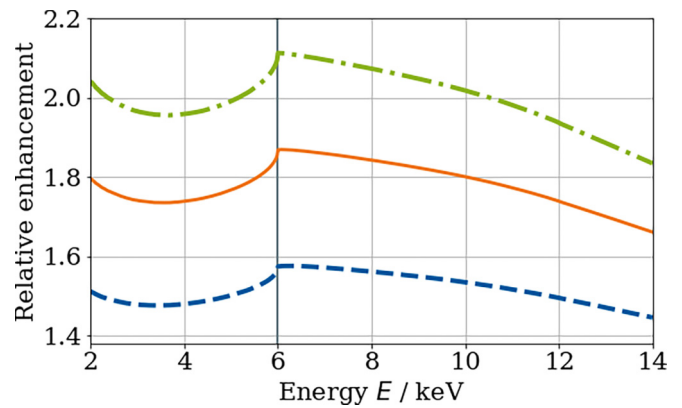


FIG. 5. Relative enhancement in the particle transmission probability in a truncated Coulomb potential (23) with vanishing offset $V_1 = 0$ as a function of initial energy E for $\omega = 6$ keV, plotted for three different field strengths \mathcal{E}_0 (green, dot-dashed: 2.0×10^{17} V/m; orange, solid: 1.8×10^{17} V/m; blue, dashed: 1.5×10^{17} V/m). Again, at $E = \omega$ (vertical, gray line) resonance peaks are found. Sufficiently away from the peaks, the relative enhancement of the transmission probability decreases with energy E .

process. If further processes such as cluster formation or many-particle tunneling (e.g., cotunneling) are involved, the associated timescales may change the region of validity of the time-averaged potential approximation.

B. Resonance effects

As we have discussed in Sec. III A, resonance effects can occur at energies $E = n\omega$, where Floquet channels open up (or close). This phenomenon is not tied to the rectangular potential but can also be observed in assisted nuclear fusion, see Fig. 5 for the case of vanishing offset $V_1 = 0$. One has to be careful in interpreting these results, however, as the Coulomb potential is very asymmetric. Consequently, nonadiabatic enhancement effects caused by the front end of the barrier are suppressed due to the slow and gradual change of the potential at the outer turning point $r^* = q^2/(4\pi\epsilon_0 E)$; see also Ref. [50]. In contrast, the sharp drop of the barrier at its rear end, i.e., the inner turning point r_0 , facilitates strong nonadiabatic enhancement effects. As an intuitive picture, the Kramers-Henneberger motion $\chi(t)$ of the barrier may “push” part of the wave function out of the rear of the barrier (displacement effect). A technical discussion of the eigenvalue structure of the corresponding Schrödinger equation and its connection to resonances is further discussed in Appendix A 3.

C. Influence of offset V_1

In a realistic description of nuclear fusion, one has to further consider nuclear attraction. In its simplest form such an attraction can be incorporated into the system of equations by adding a constant depth $V_1 > 0$ in Eq. (23). Calculation of the transmission probability as a function of this parameter V_1 reveals a rich, nonmonotonic behavior, see Fig. 6.

We identify three regions. In the limit of shallow depths $V_1 < 100$ keV, the zeroth Floquet channel T_0 corresponding

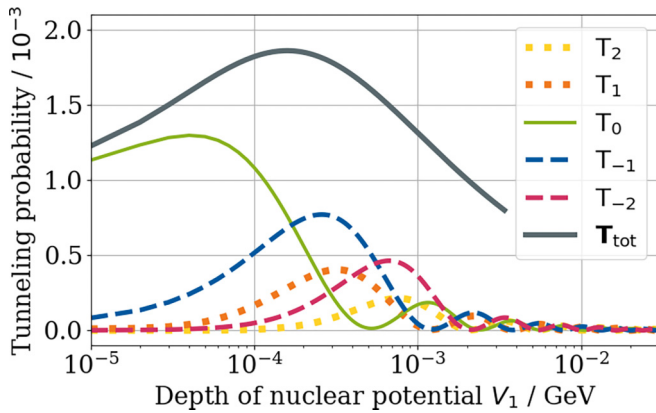


FIG. 6. Transmission probability in assisted DT fusion as a function of the depth of the attractive nuclear potential V_1 . Important individual channels are shown, indicated by their difference from the initial energy in terms of $\pm n\omega$, as well as the total transmission probability (gray, solid line). The initial particle energy is $E = 14$ keV, while the applied electric field shows a peak field strength of $\mathcal{E}_0 = 8 \times 10^{16}$ V/m at oscillation frequency $\omega = 6$ keV.

to the incident energy E yields the main contribution. In this regime the total tunneling probability increases with V_1 , but already before the maximum tunneling probability is reached, we see that this increase cannot be explained by the zeroth Floquet channel T_0 alone, i.e., the sidebands ($T_{\pm 1}$ and $T_{\pm 2}$, etc.) become important.

In the intermediate regime between 100 keV and 1 MeV, the total tunneling probability assumes its maximum and starts to decrease with V_1 . At the same time, the sidebands (first $T_{\pm 1}$, then $T_{\pm 2}$, etc.) dominate the zeroth Floquet channel T_0 .

In the limit of very deep potentials $V_1 > 1$ MeV, classified as the third regime, the total tunneling probability becomes distributed over more and more Floquet channels (rendering the numerical integration increasingly difficult). The final particle energy has effectively become continuous.

D. Relative enhancement

In contrast to Fig. 6 displaying the total tunneling probability, let us now discuss the enhancement in comparison to the static case. As we have observed above, the offset V_1 plays an important role. Choosing a realistic value for V_1 , however, is not so simple. First, it should be remembered that V_1 serves as an effective toy model for nuclear attraction at small distances. Second, our analysis is effectively one dimensional, whereas the real truncated Coulomb potential (23) is three dimensional. Here we choose $V_1 = 17.6$ MeV in order to accommodate for the energy gain in DT fusion.

The energy dependence of the relative enhancement is shown in Fig. 7, where we have chosen the interval between 2 and 14 keV, which should be relevant for possible future technological applications. Consistent with the discussions in the previous section, we do not observe any (discernible) resonances. Nevertheless, the relative amplification is on the level of ten percent or more for field strengths below 10^{17} V/m. For higher field strengths, it can be even stronger, see the following section. For further technical details we refer to Appendix D.

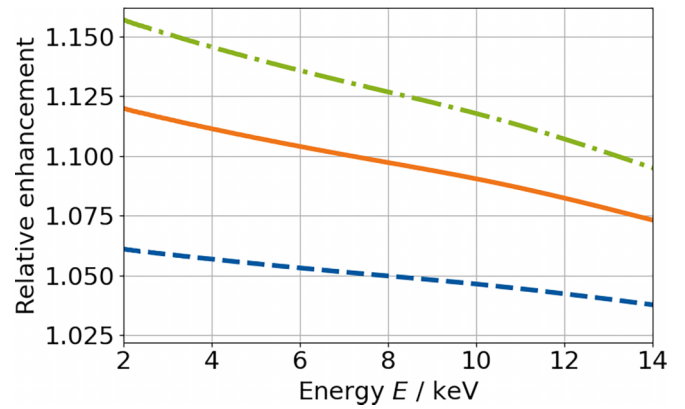


FIG. 7. Relative enhancement in the total particle transmission probability through the truncated Coulomb barrier as a function of initial energy E displayed for a variety of external field strengths \mathcal{E}_0 (dashed blue: 5×10^{16} V/m, solid orange: 7×10^{16} V/m, and dashed-dotted green: 8×10^{16} V/m). Due to the presence of a strong attractive potential, $V_1 = 17.6$ MeV, no discernible resonances around the quiver frequency $\omega = 6$ keV occur. The overall enhancement effect is nevertheless about 10%.

V. CONCLUSION

We have studied the enhancement of Schrödinger tunneling through a one-dimensional static potential barrier $V(x)$ induced by a time-dependent electric field $\mathcal{E}(t)$ that is harmonically oscillating with frequency ω . After transforming to the Kramers-Henneberger frame, we have derived and solved the equations for the Floquet channels which determine the transmission and reflection amplitudes.

As a first example we studied the rectangular potential, which can be considered as a one-dimensional toy model for a scanning tunneling microscope, or tunneling through an insulating layer between two conductors. Due to its simple structure, the results for the rectangular potential can be benchmarked with analytical approximations (e.g., in the thin-barrier as well as the opaque-barrier regime). We found resonances in the tunneling probability, e.g., at $E = \omega$ and $E = 2\omega$, i.e., when Floquet channels open (or close). These resonances are pure nonadiabatic effects and clearly show that neither the static potential approximation nor the time-averaged potential approximation are applicable in these cases.

As a second example we investigated the truncated Coulomb potential relevant for nuclear fusion, where we again found that the time-averaged potential approximation is not applicable for the parameters under consideration. Even though one can in principle also observe resonances in this scenario, they are suppressed by the gradual change of the potential at the outer turning point and the large potential drop or offset at the inner turning point. Nevertheless, for field strengths of the order of 10^{17} V/m, one can observe a significant enhancement of the tunneling probability, see Fig. 8.

In conclusion, the results of field-induced quantum tunneling look promising and encourage further research in the field of dynamical assistance. Furthermore, there is an apparent universality of quantum tunneling in oscillating electric fields

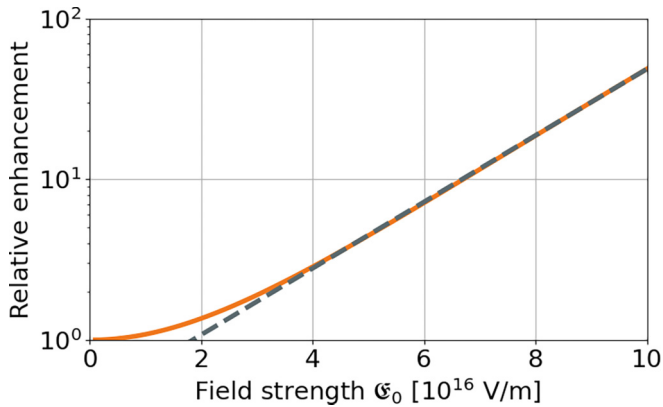


FIG. 8. Relative enhancement in the total particle transmission probability as a function of field strength \mathcal{E} for the truncated Coulomb potential relevant for nuclear fusion at $E = \omega = 2$ keV and $V_1 = 0$. For small field strengths, we observe an approximately quadratic growth which is consistent with lowest-order perturbation theory. For larger field strengths, however, the growth becomes exponential, which is due to the nonperturbative nature of tunneling and also indicates that lowest-order perturbation theory is no longer adequate.

across all energy scales, so this research could have beneficial spinoffs in other branches of physics.

VI. OUTLOOK

Since tunneling is ubiquitous in physics, our approach and results can be applied or generalized to many other cases and in several directions. For example, while we focused on transmission, one could also consider the reflection amplitudes—such as cold neutrons scattered off a vibrating potential barrier. Not surprisingly, one also obtains resonances in this case, which have actually been measured in inelastic neutron-scattering spectra [89]. The fact that these experiments have been performed in the neV regime further highlights the universality of our approach.

Note that the reflection off a vibrating potential barrier bears some similarities to the well-known mechanism of high-harmonic generation where photon beams are reflected off a plasma mirror which is set in motion by the incident laser beam; see, e.g., Refs. [90,91]. Even though the underlying wave equation is different from the Schrödinger equation considered here, the reflected beam does also consist of the incident frequency ω plus the higher-order Floquet channels $n\omega$.

As another link to existing phenomena, it would be interesting to study the relation or interplay between the resonance effects discussed here on the one hand and resonant tunneling in static (e.g., double-well) potentials $V(x)$ on the other hand; see, e.g., Refs. [92,93] for an overview. The properties of these static resonances depend sensitively on the shape of the potential $V(x)$, and adding a field $\mathcal{E}(t)$ would provide even more knobs (field strengths and driving frequency) for quantum control, e.g., quantum ratchets or spectral filters for incoming and outgoing waves separately [94–96].

Furthermore, our research may in principle also be extended to semiconductor physics. Electrons in semiconductors

are characterized by an effective mass, which can be significantly smaller than the free electron mass of 511 keV. Consequently, the energy and field strengths required to observe field-assisted quantum tunneling are substantially reduced, see Sec. III C. For instance, for a rectangular barrier and an effective mass of 50 keV, the respective field frequency for dynamically assisted transmission is in the range of 10 meV and the field strength is $\sim 5 \times 10^6$ V/m.

In general, the study of assisted quantum tunneling in three dimensions is the next objective. Then the angular momentum of the incoming wave function and, consequently, the angular momentum barrier have to be taken into account. One might turn this into an advantage, as different transitions have to be considered, such as from an incoming $l = 1$ state to an $l = 0$ state, where only the latter can effectively tunnel through the composite nuclear barrier.

Apart from the case of nonrelativistic tunneling investigated here, one can also consider relativistic tunneling. Prominent examples include false vacuum decay in early cosmology [97–100] and the Sauter-Schwinger effect, i.e., electron-positron pair creation out of the vacuum by a strong electric field [101–104]. Even though the underlying (Dirac or Klein-Fock-Gordon) equations are different from the Schrödinger equation studied here, one faces the same problem that tunneling in space-time-dependent backgrounds is not fully understood yet; see, also, Refs. [6,105–109]. On a completely different scale, these phenomena could also be related to the pseudorelativistic dynamics in graphene [110–114].

ACKNOWLEDGMENTS

Calculations have been performed on the Hemera Cluster in Dresden-Rossendorf. D.R. wants to thank Falk Adamietz for inspiring discussions. Funded by the Deutsche Forschungsgemeinschaft (DFG, German Research Foundation), Project ID No. 278162697–SFB 1242 is also gratefully acknowledged. This research was supported in part by the Perimeter Institute for Theoretical Physics. Research at the Perimeter Institute is supported by the Government of Canada through the Department of Innovation, Science and Economic Development and by the Province of Ontario through the Ontario Ministry of Research and Innovation.

APPENDIX A: THEORETICAL FORMALISM

In this section we want to detail the building blocks of the theoretical framework. This includes a full discussion of the channel equation formalism itself, as well as further explanations of how we incorporated the Kramers-Henneberger frame or a resonance study into it. Nevertheless, most of the basic derivations can be found in Refs. [115,116] and, in more detail, in Ref. [28].

1. The Kramers-Henneberger frame

The transformation from laboratory frame to Kramers-Henneberger frame is performed by means of the Kramers-Henneberger transformation. It provides an exact mapping between a vector potential $A(t)$ and a wave function's quiver motion $\chi(t)$. The starting point is the

Schrödinger equation,

$$i\hbar \frac{\partial}{\partial t} \psi(x, t) = \left(\frac{(p - qA(t))^2}{2\mu} + V(x) \right) \psi(x, t), \quad (\text{A1})$$

with a purely time-dependent vector potential $A(t)$ and time-independent scalar potential $V(x)$. The quadratic term $\dot{\xi}(t) = q^2 A(t)^2 / (2\mu)$ can be eliminated by means of a transformation

$$\psi(x, t) \rightarrow \exp(i\xi(t)) \psi(x, t), \quad (\text{A2})$$

while the linear term $\chi(t)$ can be incorporated in a spatial quiver motion $\dot{\chi}(t) = q/\mu A(t)$ through application of the translation operator,

$$\psi(x, t) \rightarrow \exp(i\chi(t)p) \psi(x, t), \quad (\text{A3})$$

and switching to a moving frame of reference

$$x \rightarrow x + \chi(t), \quad \text{thus} \quad \partial_t \rightarrow \partial_t - \dot{\chi}(t) \partial_x. \quad (\text{A4})$$

In this way we obtain the Schrödinger equation in the Kramers-Henneberger frame

$$i\hbar \frac{\partial}{\partial t} \psi_{\text{KH}}(x, t) = \left(\frac{p^2}{2\mu} + V(x - \chi(t)) \right) \psi_{\text{KH}}(x, t). \quad (\text{A5})$$

2. General formalism for uneven asymptotic levels

We want to go into detail regarding the derivation of the system of coupled equations that has been rather superficially presented in the main text. This is done in order to have a coherent, self-contained paper.

In order to employ such potential of arbitrary asymptotic levels, we first have to tweak the basic formalism slightly. More specifically, we write for the potential in the Kramers-Henneberger frame,

$$V(x, t) = W(x, t) - V_1 \Theta(x), \quad (\text{A6})$$

where $V(x \rightarrow \infty, t) = -V_1$ and $V(x \rightarrow -\infty, t) = 0$, such that $W(x \rightarrow \pm\infty, t) = 0$. We thus split the potential into a dynamical potential $W(x, t)$ and a step function $V_1 \Theta(x)$. For the sake of clarification, in the main text we only showed the simple derivation for a potential where $V_1 = 0$.

The Schrödinger equation in the Kramers-Henneberger frame is therefore given by

$$\begin{aligned} i\hbar \frac{\partial}{\partial t} \psi_{\text{KH}}(x, t) \\ = \left[-\frac{1}{2\mu} \frac{\partial^2}{\partial x^2} + W(x - \chi(t)) - V_1 \Theta(x) \right] \psi_{\text{KH}}(x, t). \end{aligned} \quad (\text{A7})$$

Within Floquet theory the wave function as well as the potentials are decomposed into Fourier modes,

$$\psi_{\text{KH}}(x, t) = e^{-iEt} \times \sum_{n=-\infty}^{\infty} u_n(x) e^{in\omega t}, \quad (\text{A8})$$

$$W(x, t) = \sum_{n=-\infty}^{\infty} W_n(x) e^{in\omega t}, \quad (\text{A9})$$

so that we arrive at the channel equation,

$$\frac{d^2}{dx^2} u_n(x) + k_n^2(x) u_n(x) = \sum_{m=-\infty}^{\infty} w_{nm}(x) u_m(x), \quad (\text{A10})$$

with $k_n(x) \equiv k_n = \sqrt{2\mu(E + n\omega)}$ for $x < 0$ and $k_n(x) \equiv k_n^{V_1} = \sqrt{2\mu(E - V_1 + n\omega)}$ for $x \geq 0$. Furthermore, we have $w_{nm}(x) \equiv 2\mu W_{n-m}(x)$.

The formal solution to Eq. (A10) is given by

$$\begin{aligned} u_{nl}(x) &= \phi_2^n(x) \delta_{nl} \\ &+ \int_{-\infty}^{\infty} dx' G_n(x, x') \times \sum_m w_{nm}(x') u_{ml}(x'), \end{aligned} \quad (\text{A11})$$

with Green's function

$$G_n(x, x') = C_n \begin{cases} \phi_1^n(x) \phi_2^n(x') & \text{for } x < x', \\ \phi_2^n(x) \phi_1^n(x') & \text{for } x > x', \end{cases} \quad (\text{A12})$$

and $C_n = -i/(k_n + k_n^{V_1})$.

The free wave functions, in turn, are given by

$$\begin{aligned} \phi_1^n(x) &= e^{-ik_n x} \Theta(-x) \\ &+ \left\{ \frac{1}{2} \left(1 - \frac{k_n}{k_n^{V_1}} \right) e^{ik_n^{V_1} x} + \frac{1}{2} \left(1 + \frac{k_n}{k_n^{V_1}} \right) e^{-ik_n x} \right\} \Theta(x), \end{aligned} \quad (\text{A13})$$

$$\phi_2^n(x) = e^{ik_n^{V_1} x} \Theta(x)$$

$$\begin{aligned} &+ \left\{ \frac{1}{2} \left(1 + \frac{k_n^{V_1}}{k_n} \right) e^{ik_n x} + \frac{1}{2} \left(1 - \frac{k_n^{V_1}}{k_n} \right) e^{-ik_n x} \right\} \Theta(-x). \end{aligned} \quad (\text{A14})$$

In the asymptotic limits we find the solutions

$$u_{nl}(x \rightarrow -\infty) = \phi_2^n(x) \delta_{nl} + \rho_{nl} \phi_1^n(x), \quad (\text{A15})$$

$$u_{nl}(x \rightarrow +\infty) = \phi_2^n(x) \delta_{nl} + \tau_{nl} \phi_2^n(x), \quad (\text{A16})$$

where

$$\rho_{nl} = C_n \int_{-\infty}^{\infty} dx' \phi_2^n(x') \times \sum_m w_{nm}(x') u_{ml}(x'), \quad (\text{A17})$$

$$\tau_{nl} = C_n \int_{-\infty}^{\infty} dx' \phi_1^n(x') \times \sum_m w_{nm}(x') u_{ml}(x'). \quad (\text{A18})$$

Rather than solving for the wave function $u_{nl}(x)$, we will derive a system of differential equations from which τ_{nl} and ρ_{nl} can be obtained directly. To do this we first generalize the formal solution (A11) to

$$\begin{aligned} u_{nl}(x, y) &= \phi_2^n(x) \delta_{nl} \\ &+ \int_y^{\infty} dx' G_n(x, x') \sum_m w_{nm}(x') u_{ml}(x', y). \end{aligned} \quad (\text{A19})$$

By taking the derivative with respect to y and multiplying Eq. (A19) with a yet undetermined matrix B we then obtain the relation

$$\begin{aligned} \sum_l \frac{\partial u_{nl}(x, y)}{\partial y} B_{ls}(y) \\ = - \sum_{l,m} C_n \phi_2^n(x) \phi_1^n(y) w_{nm}(y) u_{ml}(y, y) B_{ls}(y) \\ + \int_y^{\infty} dx' G_n(x, x') \sum_{l,m} w_{nm}(x') \frac{\partial u_{ml}(x', y)}{\partial y} B_{ls}(y). \end{aligned} \quad (\text{A20})$$

If we require the newly introduced matrix B to satisfy

$$-\sum_{l,m} C_n \phi_1^n(y) w_{nm}(y) u_{ml}(y, y) B_{ls}(y) = \delta_{ns}, \quad (\text{A21})$$

we find that Eq. (A20) is equivalent to Eq. (A19) under the relation

$$\sum_l \frac{\partial u_{ml}(x, y)}{\partial y} B_{ls}(y) = u_{ms}(x, y). \quad (\text{A22})$$

In the next step we consider the generalized amplitudes

$$\rho_{nl}(y) = C_n \int_y^\infty dx' \phi_2^n(x') \sum_m w_{nm}(x') u_{ml}(x', y), \quad (\text{A23})$$

$$\tau_{nl}(y) = C_n \int_y^\infty dx' \phi_1^n(x') \sum_m w_{nm}(x') u_{ml}(x', y). \quad (\text{A24})$$

Taking the derivative with respect to y and using the relation stated in Eq. (A21), we obtain

$$\begin{aligned} \frac{d\rho_{nl}(y)}{dy} &= -C_n \phi_2^n(y) \sum_m w_{nm}(y) u_{ml}(y, y) \\ &\quad + \sum_s \rho_{ns}(y) B_{sl}^{-1}(y), \end{aligned} \quad (\text{A25})$$

$$\begin{aligned} \frac{d\tau_{nl}(y)}{dy} &= -C_n \phi_1^n(y) \sum_m w_{nm}(y) u_{ml}(y, y) \\ &\quad + \sum_s \tau_{ns}(y) B_{sl}^{-1}(y). \end{aligned} \quad (\text{A26})$$

The inverse of the matrix B reads

$$B_{sl}^{-1}(y) = -C_s \phi_1^s(y) \sum_m w_{sm}(y) u_{ml}(y, y), \quad (\text{A27})$$

whereas from the formal solution (A19) we obtain

$$u_{ml}(y, y) = \phi_2^m(y) \delta_{ml} + \phi_1^m(y) \rho_{ml}(y). \quad (\text{A28})$$

By inserting these identities (A27)–(A28) into the set of differential equations (A25)–(A26), we finally find

$$\begin{aligned} \frac{d\rho_{nl}(y)}{dy} &= -\sum_{s,m} C_s [\phi_2^s(y) \delta_{ns} + \rho_{ns}(y) \phi_1^s(y)] \\ &\quad \times w_{sm}(y) [\phi_2^m(y) \delta_{ml} + \rho_{ml}(y) \phi_1^m(y)], \end{aligned} \quad (\text{A29})$$

$$\begin{aligned} \frac{d\tau_{nl}(y)}{dy} &= -\sum_{s,m} C_s [\phi_1^s(y) \delta_{ns} + \tau_{ns}(y) \phi_1^s(y)] \\ &\quad \times w_{sm}(y) [\phi_2^m(y) \delta_{ml} + \rho_{ml}(y) \phi_1^m(y)]. \end{aligned} \quad (\text{A30})$$

This set of equations has to be integrated from $y \rightarrow \infty$ to $y \rightarrow -\infty$. Initial conditions are given by

$$\rho_{nl}(y \rightarrow \infty) = 0, \quad \tau_{nl}(y \rightarrow \infty) = 0. \quad (\text{A31})$$

Reflection and transmission amplitudes are identified as

$$R_{nl} = \rho_{nl}(y \rightarrow -\infty), \quad (\text{A32})$$

$$T_{nl} = \delta_{nl} + \tau_{nl} = \delta_{nl} + \tau_{nl}(y \rightarrow -\infty). \quad (\text{A33})$$

In the presentation in the main text we opted for a more comprehensive representation that is easier to follow. In order

to recover the simplified version, we have to have a potential that truly vanishes asymptotically, as then $k_s^{V_1}$ is equal to k_s , and thus $C_s = -i/(k_s + k_s^{V_1})$, and $w_{sm}(y)$ is reduced to $v_{sm}(y)$. For the wave functions ϕ_1 and ϕ_2 , an expansion in terms of plane waves further yields $\phi_2^s(y) = e^{ik_s y}$ and $\phi_1^s(y) = e^{-ik_s y}$, respectively, completing the translation.

3. Resonances

In order to confirm the presence of resonances in the transmission probability we rely on techniques developed in a non-Hermitian formulation of quantum mechanics; see Ref. [117] for an overview. In the context of an analysis of quantum tunneling through the complex domain see also Refs. [118–120]. For our study we search for solutions in the Floquet-Schrödinger equation (10) by performing a scaling transformation $x \rightarrow x e^{i\theta}$, where θ is a real constant:

$$\frac{d^2}{dx^2} u_n(x) + 2\mu(\mathcal{E} + n\omega) u_n(x) = \sum_{m=-\infty}^{\infty} v_{nm}(x) u_m(x). \quad (\text{A34})$$

In this case $v_{nm}(x) \equiv 2\mu V_{n-m}(x)$, which expands the solution space to the complex plane. Consequently, the only normalizable solutions in energy are to be found in the complex plane. We indicate this shift by writing \mathcal{E} instead of E .

As a matter of fact, we expect the complex solutions \mathcal{E} to be localized either along straight lines (under an angle α depending on the chosen value of θ measuring the tilt from the real x axis) or at isolated points. To better visualize the former aspect conceptually, we want to consider the limit of a decoupled set of equations, that is where $v_{nm} = 0$. In this case the Floquet-Schrödinger equation reduces to a simple eigenwert equation:

$$\left(-\frac{e^{-2i\theta}}{2\mu} \frac{d^2}{dx^2} - n\omega \right) u_n(x) = \mathcal{E} u_n(x). \quad (\text{A35})$$

Solutions in $u_n(x)$ are of the form $\sim \exp(ikx e^{-i\theta})$ and demanding these eigenvectors to be normalizable we find the necessary condition $k = |k| e^{i\theta}$. Consequently, the eigenvalues are given by

$$\mathcal{E} = -n\omega + |k|^2 e^{-2i\theta}. \quad (\text{A36})$$

Resonances only appear if the wave function is coupled to a quivering potential, and hence not all v_{nm} vanish. Solutions of \mathcal{E} that do not follow the simple relation (A36) can therefore be associated with the resonant enhancement we see in the transmission probability.

In Fig. 9 an exemplary plot of the imaginary eigenvalue landscape of the shifted Schrödinger equation is displayed. Of interest are the locations of the isolated points, as they mark the existence of resonances. Such isolated points appear at real energies of zero, 6 keV, 12 keV, and so on. They are also (almost) independent of the shift parameter θ , in contrast to the regular spectrum which builds out tilted line structures.

APPENDIX B: RECTANGULAR BARRIER

In this section the solutions for field-induced quantum tunneling through a rectangular barrier are presented. We also

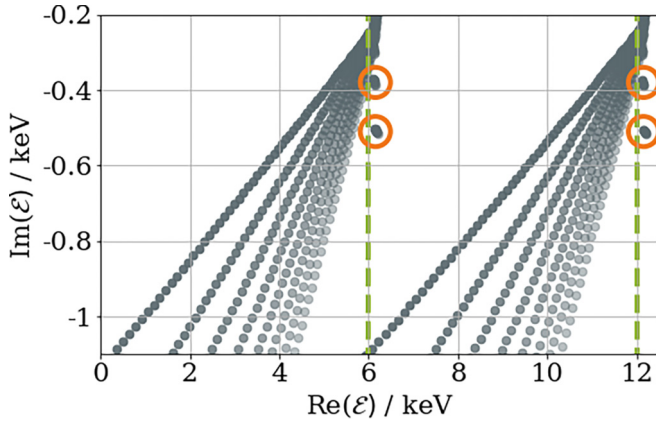


FIG. 9. Eigenvalue structure of the Schrödinger equation for the Coulomb potential in the complex energy plane \mathcal{E} for different values of θ . The singular points, highlighted through orange circles, mark the onset of a resonance. These locations coincide with the frequency of the applied field ω (green, dashed lines), which for this specific example, was chosen to be $\omega = 6$ keV. The lines of gray dots mark branch cuts, which simply refer to the regular spectrum in the continuum. The field strength was fixed at $\mathcal{E}_0 = 3 \times 10^{16}$ V/m.

give an outlook regarding an analytical solution for such tunneling with an electric field present.

$$r_E = \frac{(k_I - k_{II})(k_{II} + k_{III}) + (k_I + k_{II})(k_{II} - k_{III})e^{2ik_{II}L}}{(k_I + k_{II})(k_{II} + k_{III}) + (k_I - k_{II})(k_{II} - k_{III})e^{2ik_{II}L}}, \quad (\text{B2})$$

$$t_E = -\frac{4k_I k_{II} e^{iL(k_{II} - k_{III})}}{-(k_I + k_{II})(k_{II} + k_{III}) + (k_{II} - k_I)(k_{II} - k_{III})e^{2ik_{II}L}}, \quad (\text{B3})$$

with

$$k_I = \sqrt{2\mu E}, \quad k_{II} = \sqrt{2\mu(E - V_0)} \\ \text{and } k_{III} = \sqrt{2\mu(E + V_1)}. \quad (\text{B4})$$

Reflection R and transmission probabilities T are then obtained through conservation of the total probability current

$$1 = R + T = |r_E|^2 + \sqrt{1 + V_1/E} |t_E|^2. \quad (\text{B5})$$

Note that the prefactor $\sqrt{1 + V_1/E}$ increases with a larger potential depth in region III. If $V_1 \gg E$ the wave is thus effectively reflected at the second boundary.

2. Quivering barrier

In this section we consider tunneling through a quivering rectangular potential, see Eq. (B1). Due to its special shape, the potential is locally constant in each region. An analytical solution for the reflection and transmission rate can even be found for tunneling with an additional oscillating electric field present. The procedure, while more involved, is the same as for the textbook example of tunneling through a static barrier; see also the derivation above. Nevertheless, we present the underlying concept in the following.

1. Static barrier

Obtaining the transmission rates for particle tunneling through a rectangular barrier is one of the textbook examples of quantum mechanics. If, however, the potential in front of and behind the barrier is not on the same level, the results for the transmission rates are already much less well known. For the sake of providing a complete picture of our analysis on field-assisted quantum tunneling, we thus state the overall strategy for finding analytical solutions and also provide various sample results, e.g., for a rectangular barrier on uneven ground.

In terms of scattering at a rectangular barrier we find three regions,

$$V(x) = \begin{cases} 0 & \text{for } x \leq 0, \\ V_0 > 0 & \text{for } 0 \leq x \leq L, \\ -V_1 < 0 & \text{for } x \geq L, \end{cases} \quad (\text{B1})$$

which we will denote according to their appearance in Eq. (B1) as region I, region II, and region III, respectively. Equivalently to the textbook case, we make an ansatz for the wave function, dividing it into three segments with a left- and right-moving part in each segment. The main difference is that we have three distinct wave numbers k_I , k_{II} , and k_{III} , one for each region. For our purposes we demand $-V_1 < 0 < E < V_0$ and have the wave function propagate from left to right. We then obtain for reflection r_E and transmission t_E rates

The starting point is again the Schrödinger equation, see Eq. (A1):

$$i\hbar \frac{\partial}{\partial t} \psi(x, t) = \left(\frac{(p - qA(t))^2}{2\mu} + V(x) \right) \psi(x, t), \quad (\text{B6})$$

with vector potential $A(t)$. As $A(t) = -\mathcal{E}_0/\omega \sin(\omega t)$ is periodic, so is the quiver motion $\chi(t) = q\mathcal{E}_0/\mu\omega^2 \cos(\omega t)$ with amplitude $\chi_0 = q\mathcal{E}_0/\mu\omega^2$ and, in turn, the translation operator. Then, when applying the translation operator to make the transition to a moving frame, the solutions to the Schrödinger equations are again provided in terms of region-specific wave functions:

$$\psi_I = e^{-iEt + ik_{I0}X(t)} + \sum_m A_m^l e^{-i(E+m\omega)t - ik_{Im}X(t)}, \quad (\text{B7})$$

$$\psi_{II} = \sum_m B_m^r e^{-i(E+m\omega)t + ik_{II}X(t)} + \sum_m B_m^l e^{-i(E+m\omega)t - ik_{II}X(t)}, \quad (\text{B8})$$

$$\psi_{III} = \sum_m C_m^r e^{-i(E+m\omega)t + ik_{III}X(t)}, \quad (\text{B9})$$

with $X(t) = x + \chi(t)$. Each wave function is given in terms of its Fourier decomposition and with respect to the general

time evolution in the Schrödinger equation,

$$\psi(x, t) = e^{-iEt} \sum_{n=-\infty}^{\infty} \phi_n(x) e^{im\omega t}, \quad (\text{B10})$$

with generic $\phi(x)$ used as a stand-in for the left- and right-propagating waves in all three regions. If the amplitude of the quivering motion is set to zero, all $\phi_m(x)$ with $m \neq 0$ vanish. Thus the time translation factors out, and the familiar structure for static tunneling is recovered as wave vectors simplify:

$$k_{\text{Im}} = \sqrt{2\mu(E + m\omega)}, \quad k_{\text{II}m} = \sqrt{2\mu(E + m\omega - V_0)},$$

and $k_{\text{III}m} = \sqrt{2\mu(E + m\omega + V_1)}$. (B11)

Also note that in the above ansatz we have already incorporated appropriate initial conditions, in particular, there is one and only one incoming mode $A_0^r = 1$, and thus $A_{m \neq 0}^r = 0$ and $C_m^l = 0$.

Furthermore, due to the fact that the potential oscillates, we can use the identity

$$e^{a \cos(\omega t)} = \sum_n f_n(a) e^{in\omega t} \quad (\text{B12})$$

for the χ -dependent part of the wave functions. This allows us to use the relation

$$f_n(a) = \frac{\omega}{2\pi} \int_0^{2\pi/\omega} dt e^{a \cos(\omega t) - in\omega t} = I_n(a), \quad (\text{B13})$$

where $I_n(a)$ are the modified Bessel functions of the first kind.

Junction conditions at $x = 0$ and $x = L$ then yield the algebraic equations

$$\begin{aligned} I_n(ik_{\text{I}0}\chi_0) + \sum_m I_{n+m}(-ik_{\text{Im}}\chi_0)A_m^l \\ = \sum_m I_{n+m}(ik_{\text{II}m}\chi_0)B_m^r \\ + \sum_m I_{n+m}(-ik_{\text{III}m}\chi_0)B_m^l, \end{aligned} \quad (\text{B14})$$

$$\begin{aligned} ik_{\text{I}0}I_n(ik_{\text{I}0}\chi_0) - \sum_m ik_{\text{Im}}I_{n+m}(-ik_{\text{Im}}\chi_0)A_m^l \\ = \sum_m ik_{\text{II}m}I_{n+m}(ik_{\text{II}m}\chi_0)B_m^r \\ - \sum_m ik_{\text{III}m}I_{n+m}(-ik_{\text{III}m}\chi_0)B_m^l, \end{aligned} \quad (\text{B15})$$

$$\begin{aligned} \sum_m I_{n+m}(ik_{\text{II}m}\chi_0)B_m^r e^{ik_{\text{II}m}L} \\ + \sum_m I_{n+m}(-ik_{\text{III}m}\chi_0)B_m^l e^{-ik_{\text{III}m}L} \\ = \sum_m I_{n+m}(ik_{\text{III}m}\chi_0)C_m^r e^{ik_{\text{III}m}L}, \end{aligned} \quad (\text{B16})$$

$$\begin{aligned} \sum_m ik_{\text{II}m}I_{n+m}(ik_{\text{II}m}\chi_0)B_m^r e^{ik_{\text{II}m}L} \\ - \sum_m ik_{\text{III}m}I_{n+m}(-ik_{\text{III}m}\chi_0)B_m^l e^{-ik_{\text{III}m}L} \\ = \sum_m ik_{\text{III}m}I_{n+m}(ik_{\text{III}m}\chi_0)C_m^r e^{ik_{\text{III}m}L}. \end{aligned} \quad (\text{B17})$$

This system of equations then has to be solved for the amplitudes A^l, B^l, B^r , and C^l . It is often more illuminating, however, to calculate the reflection and tunneling probabilities instead of the respective coefficients. Requiring conservation of the probability current

$$j = \frac{i}{2} \frac{\omega}{2\pi} \int_0^{2\pi/\omega} dt \left(\psi \frac{\partial}{\partial x} \psi^* - \psi^* \frac{\partial}{\partial x} \psi \right) \quad (\text{B18})$$

yields conservation of probability (normalized to 1)

$$1 = \sum_m \frac{k_{\text{Im}}}{k_{\text{I}0}} |A_m^l|^2 + \sum_m \frac{k_{\text{III}m}}{k_{\text{I}0}} |C_m^r|^2, \quad (\text{B19})$$

where the sums are over all real $k_{\text{Im}}, k_{\text{III}m}$ only.

3. Perturbative analysis

In this section we discuss field-induced quantum tunneling through a rectangular barrier in terms of perturbation theory. This is a follow-up of the derivation in the section above. The small (perturbative) parameter is $k\chi_0$, where k are again the momentum vectors in the different regions, respectively, and χ_0 is the quiver amplitude. Note that for this specific analysis we have equal asymptotic potential levels. Therefore we assume small displacements and a barrier that is moderately high compared to the incident energy V_0 in relation to E . In these conditions the arguments in the various Bessel functions I_n are small, in particular, $I_0(ik\chi_0) \approx 1$ and $I_1(ik\chi_0) \approx ik\chi_0/2$. Moreover, the mode with energy E is dominant in all regions, $|\phi_0|^2 \gg |\phi_{\pm 1}|^2$ (B10).

Performing a perturbative expansion of the wave functions (B7)–(B9) to zeroth order yields simplified junction conditions at $x = 0$,

$$1 + A_0^l = B_0^r + B_0^l, \quad (\text{B20})$$

$$ik_{\text{I}0}(1 - A_0^l) = ik_{\text{II}0}(B_0^r + B_0^l), \quad (\text{B21})$$

and $x = L$,

$$B_0^r e^{ik_{\text{II}0}L} + B_0^l e^{-ik_{\text{III}0}L} = e^{ik_{\text{I}0}L} C_0^r, \quad (\text{B22})$$

$$ik_{\text{II}0}(B_0^r e^{ik_{\text{II}0}L} - B_0^l e^{-ik_{\text{III}0}L}) = ik_{\text{I}0} e^{ik_{\text{I}0}L} C_0^r. \quad (\text{B23})$$

In the next-to-leading-order expansion we find

$$A_{\pm 1}^l = B_{\pm 1}^r + B_{\pm 1}^l, \quad (\text{B24})$$

$$-ik_{\text{II}\pm 1} A_{\pm 1}^l = \mu V_0 \chi_0 (B_0^r + B_0^l) + k_{\text{II}\pm 1} (B_{\pm 1}^r - B_{\pm 1}^l), \quad (\text{B25})$$

$$C_{\pm 1}^r e^{ik_{\text{I}\pm 1}L} = B_{\pm 1}^r e^{ik_{\text{II}\pm 1}L} + B_{\pm 1}^l e^{-ik_{\text{III}\pm 1}L}, \quad (\text{B26})$$

$$\begin{aligned} ik_{\text{I}\pm 1} C_{\pm 1}^r e^{ik_{\text{I}\pm 1}L} = \mu V_0 \chi_0 (B_0^r e^{ik_{\text{II}0}L} + B_0^l e^{-ik_{\text{III}0}L}) \\ + k_{\text{II}\pm 1} (B_{\pm 1}^r e^{ik_{\text{II}\pm 1}L} - B_0^l e^{-ik_{\text{III}\pm 1}L}), \end{aligned} \quad (\text{B27})$$

where we have already incorporated the zeroth-order terms (B20)–(B23).

In solving for the transmission amplitudes in the side channels $C_{\pm 1}^r$, we are able to establish a distinct scaling behavior. When the scalar potential becomes opaque $\sqrt{\mu V_0} L \gg 1$, the

exponential, suppressive behavior dominates. Hence the amplitude decreases over the barrier length:

$$|C_{+1}^r|^2 \approx \frac{8\mu\chi_0^2 E}{V_0} (V_0 - E - \omega) e^{-2k_{1+}L}, \quad (\text{B28})$$

$$|C_{-1}^r|^2 \approx \frac{8\mu\chi_0^2 E}{V_0} (V_0 - E) e^{-2k_{10}L}. \quad (\text{B29})$$

On the other hand, for easily transmissible barriers $\sqrt{\mu V_0}L \ll 1$ we find, under the constraint $E > \omega$, for the transmission amplitudes,

$$|C_{\pm 1}^r|^2 \approx \left(\frac{\mu V_0 L \chi_0}{2} \right)^2 \left(\frac{\sqrt{2\mu E}}{\sqrt{2\mu(E \pm \omega)}} - 1 \right)^2. \quad (\text{B30})$$

The transmitted probability currents

$$j_{\text{trans}}^{\pm 1} = \left(1 \pm \frac{\omega}{E} \right) |C_{\pm 1}^r|^2 \quad (\text{B31})$$

then satisfy the relation

$$\frac{j_{\text{trans}}^{+1}}{j_{\text{trans}}^{-1}} = \frac{\sqrt{E - \omega} (\sqrt{E + \omega} - \sqrt{E})^2}{\sqrt{E + \omega} (\sqrt{E - \omega} - \sqrt{E})^2} < 1. \quad (\text{B32})$$

Hence, for a small rectangular barrier, the transmitted current through the first upper side channel is smaller than the first lower side channel.

Furthermore, both channels have at least one maximum as a function of barrier length L . The position of these maxima can be estimated as

$$L_{\text{max}}^{\pm 1} \sim \frac{1}{\sqrt{2\mu(V_0 - E \mp \omega)}}. \quad (\text{B33})$$

As we see, the position of this maximum is different for lower and upper channels, respectively.

4. Opaque-barrier approximation

We start with a general ansatz for the transmitted wave function

$$\psi(x, t) = \int dE \psi_{\text{trans}}(E) e^{-iEt + i\sqrt{2\mu E}(x - \chi(t))}, \quad (\text{B34})$$

with quiver motion $\chi(t)$. For an incoming test energy E_{in} we find within the opaque-barrier approximation ($V_0 \gg \omega$, $V_0 \gg E_{\text{in}}$, $L \gg \chi_0$) for the Fourier coefficients

$$\begin{aligned} \psi_{\text{trans}}(E) &\approx 4 \sqrt{\frac{E_{\text{in}}}{V_0}} e^{-\sqrt{2\mu V_0}L + i\varpi} e^{-i\sqrt{2\mu E}L} \\ &\times \int \frac{dt}{2\pi} e^{i(E - E_{\text{in}})t} e^{\sqrt{2\mu V_0}(\chi(t + i\varpi) - \chi(t))}, \end{aligned} \quad (\text{B35})$$

where in this specific case the Landauer-Büttiker time [49] takes on the form

$$\varpi = L \sqrt{\frac{\mu}{2V_0}}. \quad (\text{B36})$$

Due to the fact that the last term in the equations is again time-periodic, we can apply a Fourier decomposition

$$e^{\sqrt{2\mu V_0}(\chi(t + i\varpi) - \chi(t))} = \sum_m \phi_m e^{-im\omega t}, \quad (\text{B37})$$

with weights

$$\begin{aligned} \phi_m &= \frac{\omega}{2\pi} \int_0^{\frac{2\pi}{\omega}} dt e^{im\omega t} e^{\sqrt{2\mu V_0}(\chi(t + i\varpi) - \chi(t))} = \left(\frac{e^{\omega\varpi} - 1}{e^{-\omega\varpi} - 1} \right)^{\frac{m}{2}} \\ &\times I_m(|\chi_0| \sqrt{2\mu V_0} (e^{\omega\varpi} - 1)(e^{-\omega\varpi} - 1)), \end{aligned} \quad (\text{B38})$$

where I_m are Bessel functions of the first kind. On this basis we can perform the time integration and write

$$\psi_{\text{trans}}(E) \approx \psi_{\text{trans}}^0 \sum_m \delta(E - E_{\text{in}} - m\omega) \phi_m, \quad (\text{B39})$$

with the bare wave function

$$\psi_{\text{trans}}^0 = 4 \sqrt{\frac{E_{\text{in}}}{V_0}} e^{-\sqrt{2\mu V_0}L + E_{\text{in}}\varpi} e^{-i\sqrt{2\mu E}L}. \quad (\text{B40})$$

Consequently, we find for the transmitted probability currents

$$j_{\text{trans}}^m = \frac{k_m}{k_0} |\psi_{\text{trans}} \phi_m|^2, \quad (\text{B41})$$

with $k_m = \sqrt{2\mu(E_{\text{in}} + m\omega)}$.

At this point a comparison with the perturbative approach, Sec. B 3, is in order. The Bessel function in Eq. (B38) evaluated for small arguments yields

$$\phi_m \approx \frac{(\chi_0 \sqrt{2\mu V_0})^{|m|}}{2^{|m|} |m|!} \times (e^{\omega\varpi} - 1)^{\frac{m}{2} + \frac{|m|}{2}} (e^{-\omega\varpi} - 1)^{-\frac{m}{2} + \frac{|m|}{2}}. \quad (\text{B42})$$

In the limit of large L and $m = 1$ (first upper sideband) we obtain $\phi_m \sim e^{m\omega\varpi}$. The amplitude squared of Eq. (B39) already taking into account the δ function thus scales as $\propto e^{-2L(\sqrt{2\mu V_0} - (E + \omega)\sqrt{\mu/V_0})}$. Correspondingly, for large L and $m = -1$ (first lower sideband) we find a scaling of $\propto e^{-2L(\sqrt{2\mu V_0} - E\sqrt{\mu/V_0})}$. These results agree very well with the perturbatively calculated probabilities in Eq. (B29), provided that the momentum vector k is expanded in a Taylor series.

APPENDIX C: TRUNCATED 1/R POTENTIAL

As we are also discussing nuclear fusion, that is essentially tunneling transmission through a Coulomb barrier, it is educational to present the analytical solution for static tunneling. Equations for field-assisted quantum tunneling can, in principle, also be derived in the same way.

Again, the starting point for the derivation is the Schrödinger equation, which for a general Coulomb potential takes on the form

$$\left(-\frac{1}{2\mu} \frac{d^2}{dx^2} + \frac{\alpha}{x} \right) \psi(x) = E \psi(x), \quad (\text{C1})$$

where the fine-structure constant $\alpha = (q^2 q_1 q_2)/(4\pi \epsilon_0)$ controls the strength of the potential. In the context of nuclear fusion, this control parameter would take on the value for the fine-structure constant α times a charge factor. The solutions for tunneling and reflection amplitudes for a particle of energy E in a $1/r$ potential is given in terms of Whittaker functions \mathcal{W} . Specifically, we have for the wave function at the inner turning point r_0 that is where we truncate the $1/r$ potential to

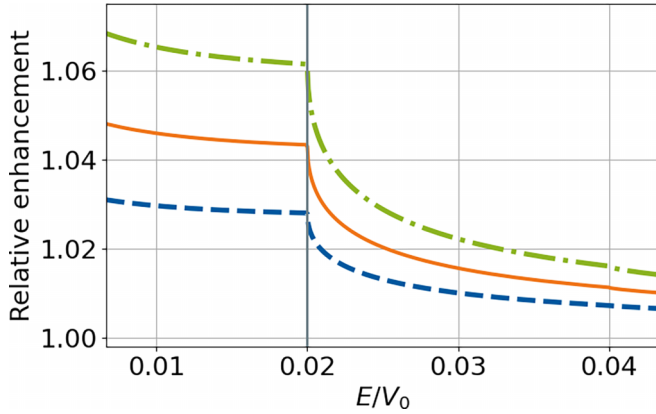


FIG. 10. Relative enhancement in the electron transmission probability through a rectangular barrier as a function of initial energy E for different external field strengths \mathcal{E}_0 (1.6×10^8 V/m for the blue dashed line, 2.0×10^8 V/m for the orange solid line, and 2.4×10^8 V/m for the green dot-dashed line). The quiver frequency is fixed to $\omega = 0.12$ eV, the barrier height is $V_0 = 6$ eV, the barrier width $L = 0.2$ nm, and the asymptotic potential behind the barrier is $V_1 = 352$ eV. In terms of dimensionless parameters we find $\omega/V_0 = 0.02$, $V_1/V_0 = 59$, $L = 2.45/\sqrt{2\mu V_0}$, and field strengths $\mathcal{E}_0 = 0.005V_0/(qL)$ (blue), $\mathcal{E}_0 = 0.0065V_0/(qL)$ (orange), and $\mathcal{E}_0 = 0.008V_0/(qL)$ (green).

keep the potential finite,

$$\psi(x) = c_E^* v_E^*(x) + r_E c_E v_E(x), \quad (C2)$$

with functions

$$v_E(x) = \mathcal{W} \left(-iV_0 \sqrt{\frac{\mu}{2E}}, 1/2, -2i\sqrt{2\mu E}x \right), \quad (C3)$$

$$c_E = (-2i\sqrt{2\mu E})^{iV_0\sqrt{\mu/2E}}, \quad (C4)$$

and reflection coefficient

$$r_E = -\frac{c_E^* \frac{dv_E^*(x)}{dx} + i\sqrt{2\mu E}v_E^*(x)}{c_E \frac{dv_E(x)}{dx} + i\sqrt{2\mu E}v_E(x)} \Big|_{x=r_0}. \quad (C5)$$

The transmission coefficient t_E is accordingly given by

$$t_E = c_E^* v_E^*(x) + r_E(x) c_E v_E(x) \Big|_{x=r_0}. \quad (C6)$$

APPENDIX D: SUPPLEMENTAL FIGURES

Finally, we would like to present additional sets of data in the form of auxiliary figures. These are used to provide additional context to our discussions, as they allow us to highlight certain details that are less suited for a general audience.

1. Rectangular barrier

In Fig. 10 the relative enhancement in the total tunneling probability is shown for strongly attractive asymptotic potential. If the initial energy E is higher than the quiver frequency ω , the relative enhancement diminishes.

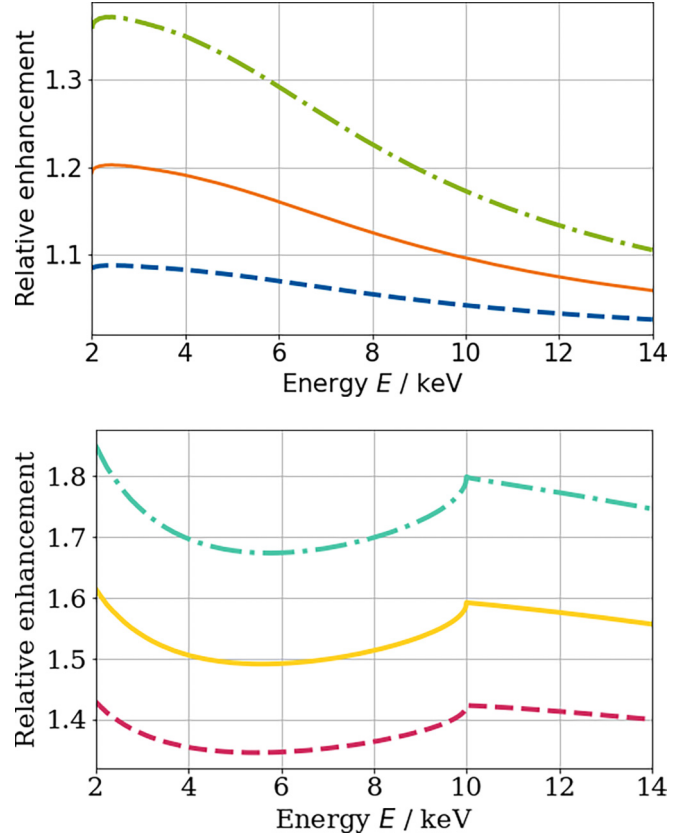


FIG. 11. Relative enhancement in particle transmission probability in a truncated Coulomb potential, with $V_1 = 0$ as a function of initial energy E for frequency $\omega = 2$ keV (top) as well as $\omega = 10$ keV (bottom). Three different field strengths have been used, respectively. For the plot at the top we have $\mathcal{E}_0 = 1.0 \times 10^{16}$ V/m for the blue dashed line, $\mathcal{E}_0 = 1.5 \times 10^{16}$ V/m for the orange solid line, and 2.0×10^{16} V/m for the green dot-dashed line. For the plot at the bottom we have $\mathcal{E}_0 = 3.0 \times 10^{17}$ V/m for the magenta dashed line, $\mathcal{E}_0 = 3.5 \times 10^{17}$ V/m for the yellow solid line, and 4.0×10^{17} V/m for the cyan dot-dashed line. An overall increase in the transmission probability the smaller the initial energy is chosen, accompanied by a resonant amplification when $E - \omega \approx 0$. In all plots the asymptotic potential levels have been fixed to zero.

2. Coulomb barrier

In Fig. 11 a Coulomb potential with equal asymptotic levels moving laterally gives rise to resonant behavior in the relative tunneling probability. These plots accompany the figure in the main text, see Fig. 5, showing that the peak position indeed varies with the quiver frequency ω .

In Fig. 12 the relative enhancement in tunneling transmission is displayed as a function of the initial energy but for varying asymptotic potential levels. The resonance structure appears if $E = n\omega + V_1$, with particle energy E , potential height V_1 , and frequency ω . If V_1 is smaller than the potential at the side of the incoming particle, the resonances are shifted to the left to smaller energies. If, on the other hand, the potential features a level $V_1 > 0$, the curve shifts to the right. Note that there is another resonance when the initial energy coincides with V_1 . But here the relative enhancement is too strong to plot, so we decided to only show the peaks at $n = 1$.

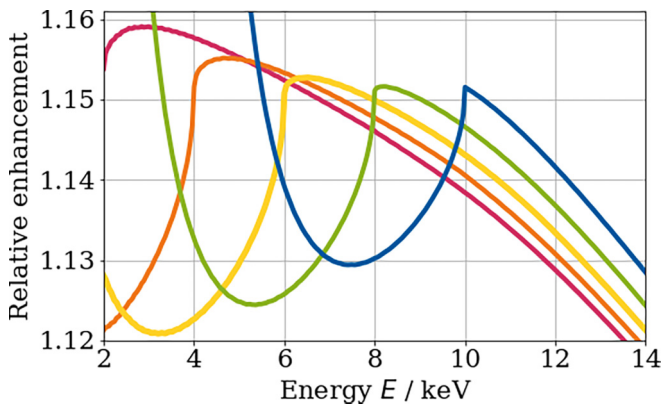


FIG. 12. Relative enhancement in the tunneling probability as a function of the initial energy E and for various potential depths V_1 in a truncated Coulomb potential. Peaks in the curves coincide with $E + n\omega = -V_1$ for $n < 0$. The quiver frequency is $\omega = 6$ keV. The field strength was fixed at $\mathcal{E}_0 \approx 8 \times 10^{16}$ V/m. Potential depths are color coded as $-V_1 = 4$ keV (blue), $-V_1 = 2$ keV (green), $-V_1 = 0$ keV (yellow), $-V_1 = 4$ keV (orange), and $-V_1 = -4$ keV (magenta).

In Fig. 13 we display the total transmission probability in a Coulomb potential as a function of a particle's initial energy for various field strengths. Overall, having an electric field boosts the transmission probability, which in

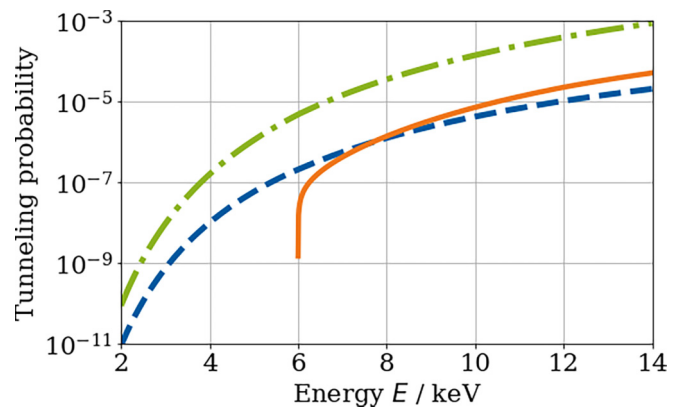


FIG. 13. Log-linear plot of the tunneling probability in a truncated Coulomb potential as a function of the initial energy E displayed in terms of the main channel (green, dot-dashed), as well as first upper (blue) and first lower (orange) side channel. The field frequency is $\omega = 6$ keV and the field strength $\mathcal{E}_0 = 10^{17}$ V/m. Lower-energy sidebands can only contribute if their final energy is above the potential's asymptotic level, here $V_1 = 0$.

this specific case, grows monotonically for all three energy channels. Nevertheless, there is an obvious difference in scaling behavior, especially for the two sidebands $E - \omega$ and $E + \omega$, as a particle's final net energy has to be strictly positive.

- [1] I. Bloch, Ultracold quantum gases in optical lattices, *Nat. Phys.* **1**, 23 (2005).
- [2] O. Morsch and M. Oberthaler, Dynamics of Bose-Einstein condensates in optical lattices, *Rev. Mod. Phys.* **78**, 179 (2006).
- [3] C. Sias, H. Lignier, Y. P. Singh, A. Zenesini, D. Ciampini, O. Morsch, and E. Arimondo, Observation of photon-assisted tunneling in optical lattices, *Phys. Rev. Lett.* **100**, 040404 (2008).
- [4] R. Ma, M. E. Tai, P. M. Preiss, W. S. Bakr, J. Simon, and M. Greiner, Photon-assisted tunneling in a biased strongly correlated Bose gas, *Phys. Rev. Lett.* **107**, 095301 (2011).
- [5] Q. Niu, X.-G. Zhao, G. A. Georgakis, and M. G. Raizen, Atomic Landau-Zener tunneling and Wannier-Stark ladders in optical potentials, *Phys. Rev. Lett.* **76**, 4504 (1996).
- [6] F. Queisser, P. Navez, and R. Schützhold, Sauter-Schwinger-like tunneling in tilted Bose-Hubbard lattices in the Mott phase, *Phys. Rev. A* **85**, 033625 (2012).
- [7] A. Eckardt, Colloquium: Atomic quantum gases in periodically driven optical lattices, *Rev. Mod. Phys.* **89**, 011004 (2017).
- [8] I. Bloch, J. Dalibard, and S. Nascimbène, Quantum simulations with ultracold quantum gases, *Nat. Phys.* **8**, 267 (2012).
- [9] E. O. Kane, Zener tunneling in semiconductors, *J. Phys. Chem. Solids* **12**, 181 (1960).
- [10] E. O. Kane, Theory of tunneling, *J. Appl. Phys.* **32**, 83 (1961).
- [11] C. Zener, A theory of the electrical breakdown of solid dielectrics, *Proc. R. Soc. A* **145**, 523 (1934).
- [12] W. Vandenberghe, B. Sorée, W. Magnus, and G. Groeseneken, Zener tunneling in semiconductors under nonuniform electric fields, *J. Appl. Phys.* **107**, 054520 (2010).
- [13] B. G. Streetman and S. Banerjee, *Solid State Electronic Devices* (Prentice-Hall, Upper Saddle River, NJ, 2005).
- [14] R. F. Voss and R. A. Webb, Macroscopic quantum tunneling in 1- μm Nb Josephson junctions, *Phys. Rev. Lett.* **47**, 265 (1981).
- [15] M. F. Linder, A. Lorke, and R. Schützhold, Analog Sauter-Schwinger effect in semiconductors for spacetime-dependent fields, *Phys. Rev. B* **97**, 035203 (2018).
- [16] S. L. Chin, F. Yergeau, and P. Lavigne, Tunnel ionisation of Xe in an ultra-intense CO2 laser field (10^{14} W cm^{-2}) with multiple charge creation, *J. Phys. B: At. Mol. Phys.* **18**, L213 (1985).
- [17] S. Augst, D. Strickland, D. D. Meyerhofer, S. L. Chin, and J. H. Eberly, Tunneling ionization of noble gases in a high-intensity laser field, *Phys. Rev. Lett.* **63**, 2212 (1989); **66**, 1247(E) (1991).
- [18] A. Hartung, F. Morales, M. Kunitski, K. Henrichs, A. Laucke, M. Richter, T. Jahnke, A. Kalinin, M. Schöffler, L. Ph. H. Schmidt, M. Ivanov, O. Smirnova, and R. Dörner, Electron spin polarization in strong-field ionization of xenon atoms, *Nat. Photon.* **10**, 526 (2016).
- [19] C. A. Mancuso, D. D. Hickstein, P. Grychtol, R. Knut, O. Kfir, X. M. Tong, F. Dollar, D. Zusin, M. Gopalakrishnan, C. Gentry, E. Turgut, J. L. Ellis, M. C. Chen, A. Fleischer, O. Cohen, H. C. Kapteyn, and M. M. Murnane, Strong-field ionization with two-color circularly polarized laser fields, *Phys. Rev. A* **91**, 031402(R) (2015).
- [20] L. V. Keldysh, Ionization in the field of a strong electromagnetic wave, *J. Exp. Theor. Phys.* **47**, 1945 (1964); [*Sov. Phys. JETP* **20**, 56 (1965)].
- [21] G. Gamow, Zur Quantentheorie des Atomkernes, *Z. Phys.* **51**, 204 (1928).

- [22] H. Geiger and J. M. Nuttall, The ranges of the α particles from various radioactive substances and a relation between range and period of transformation, *The London, Edinburgh, Dublin Philos. Mag. J. Sci.* **22**, 613 (1911); **23**, 439(E) (1912).
- [23] N. G. Kelkar, H. M. Castañeda, and M. Nowakowski, Quantum time scales in alpha tunneling, *Europhys. Lett.* **85**, 20006 (2009).
- [24] B. Ivlev and V. Gudkov, New enhanced tunneling in nuclear processes, *Phys. Rev. C* **69**, 037602 (2004).
- [25] B. Wu and J. Liu, Proton emission from halo nuclei induced by intense x-ray lasers, *Phys. Rev. C* **106**, 064610 (2022).
- [26] A. Krieger, K. Blaum, M. L. Bissell, N. Frömmgen, C. Geppert, M. Hammen, K. Kreim, M. Kowalska, J. Krämer, T. Neff, R. Neugart, G. Neyens, W. Nörtershäuser, C. Novotny, R. Sánchez, and D. T. Yordanov, Nuclear charge radius of ^{12}Be , *Phys. Rev. Lett.* **108**, 142501 (2012).
- [27] M. Grifoni and P. Hänggi, Driven quantum tunneling, *Phys. Rep.* **304**, 229 (1998).
- [28] M. Razavy, *Quantum Theory of Tunneling* (World Scientific, Hackensack, NJ, 2003).
- [29] A. Pálffy and S. V. Popruzhenko, Can extreme electromagnetic fields accelerate the α decay of nuclei? *Phys. Rev. Lett.* **124**, 212505 (2020).
- [30] D. S. Delion and S. A. Ghinescu, Geiger-Nuttall law for nuclei in strong electromagnetic fields, *Phys. Rev. Lett.* **119**, 202501 (2017).
- [31] D. Bai, D. Deng, and Z. Ren, Charged particle emissions in high-frequency alternative electric fields, *Nucl. Phys. A* **976**, 23 (2018).
- [32] D. P. Kis and R. Szilvasi, Three dimensional α -tunneling in intense laser fields, *J. Phys. G: Nucl. Part. Phys.* **45**, 045103 (2018).
- [33] Ş Mişicu and M. Rizea, Speeding of α decay in strong laser fields, *Open Phys.* **14**, 81 (2016).
- [34] Ş Mişicu and M. Rizea, α -Decay in ultra-intense laser fields, *J. Phys. G: Nucl. Part. Phys.* **40**, 095101 (2013).
- [35] E. Keski-Vakkuri and P. Kraus, Tunneling in a time-dependent setting, *Phys. Rev. D* **54**, 7407 (1996).
- [36] K. Takahashi and K. S. Ikeda, Instanton and noninstanton tunneling in periodically perturbed barriers: Semiclassical and quantum interpretations, *Phys. Rev. E* **86**, 056206 (2012).
- [37] K. Takahashi and K. S. Ikeda, Non-instanton tunneling: Semiclassical and quantum interpretations, *Phys. Rev. E* **84**, 026203 (2011).
- [38] J. Qi, L. Fu, and X. Wang, Nuclear fission in intense laser fields, *Phys. Rev. C* **102**, 064629 (2020).
- [39] F. Grossmann, T. Dittrich, P. Jung, and P. Hänggi, Coherent destruction of tunneling, *Phys. Rev. Lett.* **67**, 516 (1991).
- [40] M. Y. Azbel, Eigenstate assisted activation, *Phys. Rev. Lett.* **68**, 98 (1992).
- [41] J. A. Sto/vneng and A.-P. Jauho, Numerical studies of tunneling in a nonharmonic time-dependent potential, *Phys. Rev. B* **47**, 10446 (1993).
- [42] O. Brodier, P. Schlagheck, and D. Ullmo, Resonance-assisted tunneling, *Ann. Phys.* **300**, 88 (2002).
- [43] F. Großmann and P. Hänggi, Resonantly enhanced quantum decay, *Europhys. Lett.* **18**, 1 (1992).
- [44] S. Tomsovic and D. Ullmo, Chaos-assisted tunneling, *Phys. Rev. E* **50**, 145 (1994).
- [45] L. P. Kouwenhoven, S. Jauhar, J. Orenstein, P. L. McEuen, Y. Nagamune, J. Motohisa, and H. Sakaki, Observation of photon-assisted tunneling through a quantum dot, *Phys. Rev. Lett.* **73**, 3443 (1994).
- [46] C. Meyer, J. M. Elzerman, and L. P. Kouwenhoven, Photon-assisted tunneling in a carbon nanotube quantum dot, *Nano Lett.* **7**, 295 (2007).
- [47] A. Eckardt, T. Jinasundera, C. Weiss, and M. Holthaus, Analog of photon-assisted tunneling in a Bose-Einstein condensate, *Phys. Rev. Lett.* **95**, 200401 (2005).
- [48] A. Shudo and K. S. Ikeda, Complex classical trajectories and chaotic tunneling, *Phys. Rev. Lett.* **74**, 682 (1995).
- [49] M. Büttiker and R. Landauer, Traversal time for tunneling, *Phys. Rev. Lett.* **49**, 1739 (1982).
- [50] C. Kohlfürst, F. Queisser, and R. Schützhold, Dynamically assisted tunneling in the impulse regime, *Phys. Rev. Res.* **3**, 033153 (2021).
- [51] R. Ramos, D. Spierings, I. Racicot, and A. M. Steinberg, Measurement of the time spent by a tunnelling atom within the barrier region, *Nature (London)* **583**, 529 (2020).
- [52] H. G. Winful, Tunneling time, the Hartman effect, and superluminality: A proposed resolution of an old paradox, *Phys. Rep.* **436**, 1 (2006).
- [53] P. C. W. Davies, Quantum tunneling time, *Am. J. Phys.* **73**, 23 (2005).
- [54] N. Camus, E. Yakaboylu, L. Fechner, M. Klaiber, M. Laux, Y. Mi, K. Z. Hatsagortsyan, T. Pfeifer, C. H. Keitel, and R. Moshhammer, Experimental evidence for quantum tunneling time, *Phys. Rev. Lett.* **119**, 023201 (2017).
- [55] A. S. Landsman, M. Weger, J. Maurer, R. Boge, A. Ludwig, S. Heuser, C. Cirelli, L. Gallmann, and U. Keller, Ultrafast resolution of tunneling delay time, *Optica* **1**, 343 (2014).
- [56] F. Suzuki and W. G. Unruh, Numerical quantum clock simulations for measuring tunneling times, *Phys. Rev. A* **107**, 042216 (2023).
- [57] S. Coleman, The uses of instantons, in *Aspects of Symmetry* (Cambridge University Press, Cambridge, England, 1985).
- [58] F. Großmann, M. Fischer, T. Kunert, and R. Schmidt, Transmission probabilities for periodically driven barriers, *Chem. Phys.* **322**, 144 (2006).
- [59] S. Longhi, S. A. R. Horsley, and G. Della Valle, Scattering of accelerated wave packets, *Phys. Rev. A* **97**, 032122 (2018).
- [60] A. Pimpale and M. Razavy, Quantum tunneling in time-dependent potential barrier: A general formulation and some exactly solvable models, *Fortschr. Phys.* **39**, 85 (1991).
- [61] W. Elberfeld and M. Kleber, Time-dependent tunneling through thin barriers: A simple analytical solution, *Am. J. Phys.* **56**, 154 (1988).
- [62] Z. S. Gribnikov and G. I. Haddad, Time-dependent electron tunneling through time-dependent tunnel barriers, *J. Appl. Phys.* **96**, 3831 (2004).
- [63] D. W. Hone, R. Ketzmerick, and W. Kohn, Time-dependent Floquet theory and absence of an adiabatic limit, *Phys. Rev. A* **56**, 4045 (1997).
- [64] F. Queisser and R. Schützhold, Dynamically assisted nuclear fusion, *Phys. Rev. C* **100**, 041601(R) (2019).
- [65] W. Franz, Einfluß eines elektrischen Feldes auf eine optische Absorptionskante, *Z. Naturforsch. A* **13**, 484 (1958).

- [66] L. V. Keldysh, The effect of a strong electric field on the optical properties of insulating crystals, *J. Exp. Theor. Phys.* **34**, 1138 (1958); [*Sov. Phys. JETP* **7**, 20 (1958)].
- [67] W. C. Henneberger, Perturbation method for atoms in intense light beams, *Phys. Rev. Lett.* **21**, 838 (1968).
- [68] A. Pimpale, S. Holloway, and R. J. Smith, Tunnelling through moving barriers, *J. Phys. A: Math. Gen.* **24**, 3533 (1991).
- [69] W. Li and L. E. Reichl, Floquet scattering through a time-periodic potential, *Phys. Rev. B* **60**, 15732 (1999).
- [70] D. L. Haavig and R. Reifenberger, Dynamic transmission and reflection phenomena for a time-dependent rectangular potential, *Phys. Rev. B* **26**, 6408 (1982).
- [71] D. Ryndyk, *A Numerical Study of Dynamically Assisted Tunneling in Fusion Reactions*, Master thesis, Faculty of Physics at TU Dresden.
- [72] J. J. Bekx, M. L. Lindsey, S. H. Glenzer, and K. Schlesinger, Applicability of semiclassical methods for modeling laser-enhanced fusion rates in a realistic setting, *Phys. Rev. C* **105**, 054001 (2022).
- [73] X. Ribeyre, R. Capdessus, J. Wheeler, E. d’Humières, and G. Mourou, Multiscale study of high energy attosecond pulse interaction with matter and application to proton-Boron fusion, *Sci. Rep.* **12**, 4665 (2022).
- [74] J. J. Bekx, M. L. Lindsey, and K.-G. Schlesinger, Effect of nuclear charge on laser-induced fusion enhancement in advanced fusion fuels, *Phys. Rev. C* **106**, 034003 (2022).
- [75] X. Wang, Substantially enhanced deuteron-triton fusion probabilities in intense low-frequency laser fields, *Phys. Rev. C* **102**, 011601(R) (2020).
- [76] For example, ITER, JET, NIF as well as the Wendelstein 7-X; see the websites <https://www.iter.org/>, <https://euro-fusion.org/jet>, <https://lasers.llnl.gov/>, <https://www.ipp.mpg.de/wendelstein7x>.
- [77] K. M. McGuire, H. Adler, P. Alling *et al.*, Review of deuterium-tritium results from the Tokamak Fusion Test Reactor, *Phys. Plasmas* **2**, 2176 (1995).
- [78] L. Giuffrida, F. Belloni, D. Margarone, G. Petringa, G. Milluzzo, V. Scuderi, A. Velyhan, M. Rosinski, A. Picciotto, M. Kucharik, J. Dostal, R. Dudzak, J. Krasa, V. Istokskaja, R. Catalano, S. Tudisco, C. Verona, K. Jungwirth, P. Bellutti, G. Korn, and G. A. P. Cirrone, High-current stream of energetic α particles from laser-driven proton-boron fusion, *Phys. Rev. E* **101**, 013204 (2020).
- [79] D. C. Moreau, Potentiality of the proton-boron fuel for controlled thermonuclear fusion, *Nucl. Fusion* **17**, 13 (1977).
- [80] H. Hora, G. H. Miley, M. Ghoranneviss, B. Malekynia, N. Azizi, and X.-T. He, Fusion energy without radioactivity: Laser ignition of solid hydrogen-boron (11) fuel, *Energy Environ. Sci.* **3**, 478 (2010).
- [81] C. Labaune, C. Baccou, S. Depierreux, C. Goyon, G. Loisel, V. Yahia, and J. Rafelski, Fusion reactions initiated by laser-accelerated particle beams in a laser-produced plasma, *Nat. Commun.* **4**, 2506 (2013).
- [82] Various laser facilities all over the world are currently aiming at probing the strong-field sector of physics. For example, HIBEF, ELI, CILEX, CoReLS, ShenGuang-II as well as SLAC; see the websites <http://www.hibef.eu/>, <https://www.eli-beams.eu/>, <https://eli-laser.eu/>, <http://cilexsaclay.fr/>, <http://corels.ibs.re.kr/>, <http://lssf.cas.cn/en/>, <https://www.xfel.eu/>, <https://www6.slac.stanford.edu/>.
- [83] R. K. Adair, Nuclear potential well depth, *Phys. Rev.* **94**, 737 (1954).
- [84] W. Lv, H. Duan, and J. Liu, Enhanced deuterium-tritium fusion cross sections in the presence of strong electromagnetic fields, *Phys. Rev. C* **100**, 064610 (2019).
- [85] F. Queisser and R. Schützhold, Comment on “Enhanced deuterium-tritium fusion cross sections in the presence of strong electromagnetic fields,” [arXiv:2003.02661](https://arxiv.org/abs/2003.02661).
- [86] J. Grochmalicki, M. Lewenstein, and K. Rzaeewski, Stabilization of atoms in superintense laser fields: Is it real? *Phys. Rev. Lett.* **66**, 1038 (1991).
- [87] J. H. Eberly and K. C. Kulande, Atomic stabilization by superintense lasers, *Science* **262**, 1229 (1993).
- [88] M. Gavrilă, Atomic stabilization in superintense laser fields, *J. Phys. B: At. Mol. Opt. Phys.* **35**, R147 (2002).
- [89] J. Felber, R. Gähler, C. Rausch, and R. Golub, Matter waves at a vibrating surface: Transition from quantum-mechanical to classical behavior, *Phys. Rev. A* **53**, 319 (1996).
- [90] B. Dromey, M. Zepf, A. Gopal, K. Lancaster *et al.*, High harmonic generation in the relativistic limit, *Nat. Phys.* **2**, 456 (2006).
- [91] P. A. Franken, A. E. Hill, C. W. Peters, and G. Weinreich, Generation of optical harmonics, *Phys. Rev. Lett.* **7**, 118 (1961).
- [92] J. P. Sun, G. I. Haddad, P. Mazumder, and J. N. Schulman, Resonant tunneling diodes: Models and properties, *Proc. IEEE* **86**, 641 (1998).
- [93] G. Platero and R. Aguado, Photon-assisted transport in semiconductor nanostructures, *Phys. Rep.* **395**, 1 (2004).
- [94] H. Schanz, M. Otto, R. Ketzmerick, and T. Dittrich, Classical and quantum Hamiltonian ratchets, *Phys. Rev. Lett.* **87**, 070601 (2001).
- [95] P. Reimann, M. Grifoni, and P. Hänggi, Quantum ratchets, *Phys. Rev. Lett.* **79**, 10 (1997).
- [96] H. Linke, T. E. Humphrey, A. Löfgren, A. O. Sushkov, R. Newbury, R. P. Taylor, and P. Omling, Experimental tunneling ratchets, *Science* **286**, 2314 (1999).
- [97] S. Coleman, Fate of the false vacuum: Semiclassical theory, *Phys. Rev. D* **15**, 2929 (1977); **16**, 1248(E) (1977).
- [98] C. G. Callan, Jr. and S. Coleman, Fate of the false vacuum, II. First quantum corrections, *Phys. Rev. D* **16**, 1762 (1977).
- [99] J. Braden, M. C. Johnson, H. V. Peiris, A. Pontzen, and S. Weinfurter, New semiclassical picture of vacuum decay, *Phys. Rev. Lett.* **123**, 031601 (2019); **129**, 059901(E) (2022).
- [100] T. P. Billam, K. Brown, and I. G. Moss, False-vacuum decay in an ultracold spin-1 Bose gas, *Phys. Rev. A* **105**, L041301 (2022).
- [101] F. Sauter, Über das Verhalten eines Elektrons im homogenen elektrischen Feld nach der relativistischen Theorie Diracs, *Z. Phys.* **69**, 742 (1931).
- [102] J. Schwinger, On gauge invariance and vacuum polarization, *Phys. Rev.* **82**, 664 (1951).
- [103] R. Schützhold, H. Gies, and G. Dunne, Dynamically assisted Schwinger mechanism, *Phys. Rev. Lett.* **101**, 130404 (2008).
- [104] C. Kohlfürst, N. Ahmadiniaz, J. Oertel, and R. Schützhold, Sauter-Schwinger effect for colliding laser pulses, *Phys. Rev. Lett.* **129**, 241801 (2022).

- [105] A. Ilderton, Physics of adiabatic particle number in the Schwinger effect, *Phys. Rev. D* **105**, 016021 (2022).
- [106] M. Diez, R. Alkofer, and C. Kohlfürst, Identifying time scales in particle production from fields, *Phys. Lett. B* **844**, 138063 (2023).
- [107] Á. Álvarez-Domínguez, J. A. R. Cembranos, L. J. Garay, M. Martín-Benito, Á. Parra-López, and J. M. Sánchez Velázquez, Operational realization of quantum vacuum ambiguities, *Phys. Rev. D* **108**, 065008 (2023).
- [108] P. Krekora, Q. Su, and R. Grobe, Interpretational difficulties in quantum field theory, *Phys. Rev. A* **73**, 022114 (2006).
- [109] P. Krekora, Q. Su, and R. Grobe, Klein paradox in spatial and temporal resolution, *Phys. Rev. Lett.* **92**, 040406 (2004).
- [110] A. I. Berdyugin, N. Xin, H. Gao, S. Slizovskiy *et al.*, Out-of-equilibrium criticalities in graphene superlattices, *Science* **375**, 430 (2022).
- [111] A. Schmitt, P. Vallet, D. Mele, M. Rosticher, T. Taniguchi, K. Watanabe, E. Bocquillon, G. Fève, J. M. Berroir, and C. Voisin *et al.*, Mesoscopic Klein-Schwinger effect in graphene, *Nat. Phys.* **19**, 830 (2023).
- [112] R. Biswas and C. Sinha, Photon induced tunneling of electron through a graphene electrostatic barrier, *J. Appl. Phys.* **114**, 183706 (2013).
- [113] M. A. Zeb, K. Sabeeh, and M. Tahir, Chiral tunneling through a time-periodic potential in monolayer graphene, *Phys. Rev. B* **78**, 165420 (2008); **79**, 089903(E) (2009).
- [114] F. Queisser, K. Krutitsky, P. Navez, and R. Schützhold, Doublon-holon pair creation in Mott-Hubbard systems in analogy to QED, [arXiv:2305.04895](https://arxiv.org/abs/2305.04895).
- [115] W. van Dijk and M. Razavy, Collinear collision of an atom with a homonuclear diatomic molecule, *Int. J. Quantum Chem.* **16**, 1249 (1979).
- [116] W. Van Dijk and A. Modinos, Comparison of transfer Hamiltonian approximation, Born approximation and exact coefficients of inelastic electron tunnelling, *Surf. Sci.* **114**, 642 (1982).
- [117] N. Moiseyev, *Non-Hermitian Quantum Mechanics* (Cambridge University Press, Cambridge, England, 2011).
- [118] K. Takahashi and K. S. Ikeda, Anomalously long passage through a rounded-off-step potential due to a new mechanism of multidimensional tunneling, *Phys. Rev. Lett.* **97**, 240403 (2006); **107**, 219903(E) (2011).
- [119] J. P. Palomares-Báez, B. Ivlev, and J. L. Rodríguez-López, Enhanced tunneling through nonstationary barriers, *Phys. Rev. A* **76**, 052103 (2007).
- [120] T. Tanizawa, Quantum tunneling rate in oscillating fields, *J. Phys. Soc. Jpn.* **65**, 3157 (1996).